

UC Riverside

UC Riverside Electronic Theses and Dissertations

Title

Prediction and Visualization of Temperature Histories in Optically-Irradiated Cryogenic Tissues

Permalink

<https://escholarship.org/uc/item/9zb8r852>

Author

Slade, Adam Broadbent

Publication Date

2014

Peer reviewed|Thesis/dissertation

UNIVERSITY OF CALIFORNIA
RIVERSIDE

Prediction and Visualization of Temperature Histories in Optically-Irradiated Cryogenic
Tissues

A Dissertation submitted in partial satisfaction
of the requirements for the degree of

Doctor of Philosophy

in

Mechanical Engineering

by

Adam B. Slade

August 2014

Dissertation Committee:

Dr. Guillermo Aguilar, Chairperson

Dr. Masaru P. Rao

Dr. Hideaki Tsutsui

Copyright by
Adam B. Slade
2014

The Dissertation of Adam B. Slade is approved:

Committee Chairperson

University of California, Riverside

ACKNOWLEDGEMENTS

There have been many people that have contributed to the completion of this dissertation. While no single individual has made this dissertation possible (myself included), the exclusion of any one of these would have left my graduate experience lacking.

Among those I wish to acknowledge are the support staff in various capacities, and in multiple departments across campus. These individuals have been helpful in raising colonies of mice, helping me submit proposals, ordering requested supplies, fixing broken copiers, learn to use a microtome, etc.

I also acknowledge the generous financial support of various organizations that have in part supported this research, including a 2011 UC MEXUS dissertation research grant.

I have had the privilege to work and consult with a variety of individuals also involved in their own education. The graduate and post-doctoral students who quickly oriented me upon my arrival are very much appreciated. My foreign undergraduate summer students provided enthusiasm, insight, and valuable labor. My current set of colleagues provide me ongoing opportunities to learn and develop.

I acknowledge and greatly appreciate my mentoring professors, all of which have increased both my knowledge, curiosity, and desire to more fully understand the mysteries of engineering. I appreciate those willing to selflessly serve on exam

committees, and see to my progression and success. My research advisor in particular has been a constant resource to me for insight, support, and encouragement.

While not directly involved in research activities, my family has played a critical role in my well-being throughout my dissertation work. I have experienced nothing but support and encouragement considerable patience from my family. I have been blessed in particular with a wonderful wife who has enabled me to enjoy the start of our own family concurrently with the furthering of my education. The sacrifices that family has made on my behalf are awe inspiring, and serve as a reminder to me that my success is certainly not mine alone.

Additionally, I'd like to acknowledge that the whole of Chapter 3 was first published as "Green Fluorescent Protein as an Indicator of Cryoinjury in Tissues" in *Annals of Biomedical Engineering* in December 2013, Volume 41, Issue 12, pages 2676 – 2686 [1]. Also, Figure 2.1 and Figure 2.2 were first published in "Laser-Assisted Cryosurgery in ex vivo Mice Hepatic Tissue: Viability Assays Using Green Fluorescent Protein", *Annals of Biomedical Engineering* in February 2011, Volume 39, Issue 2, pages 636-648 [2]. Both of these excerpts are reproduced in this dissertation with kind permission from Springer Science and Business Media.

*Dedicated to the familial, ecclesiastical, and secular friends
who inspired, encouraged, and supported me in my pursuit of
enlightenment.*

ABSTRACT OF THE DISSERTATION

Prediction and Visualization of Temperature Histories in Optically-Irradiated Cryogenic Tissues

by

Adam B. Slade

Doctor of Philosophy, Graduate Program in Mechanical Engineering
University of California, Riverside, August 2014
Dr. Guillermo Aguilar, Chairperson

Cryosurgery is a useful technique in the selective destruction of undesirable tissues, such as tumors, within the human body. Cryosurgery's primary benefit is that as a percutaneous method, it reduces the invasiveness and cost associated with traditional surgery. The objective of cryosurgery is to ensure complete destruction of the target tissue while simultaneously minimizing collateral damage to surrounding tissues. In addition to the problem of collateral damage, the nature of cryosurgery can make it difficult to ascertain the extent of cryoinjury during the surgical procedure. The scope of this work is to provide tools to minimize collateral damage, visualize cryoinjury following cryoinsult, and to better simulate cryosurgical outcomes.

A method to counteract the collateral damage of cryosurgery was developed, which employs laser heating to thermally protect tissues surrounding a target tissue (e.g. tumor). A mouse hepatic tissue sample was cryogenically frozen with a cryoprobe on one

side of the tissue, while freezing of the other side was prevented using selective laser heating. Tissue biopsies confirmed that this method can successfully protect regions of tissue from cryogenic damage through gentle laser heating.

To visually characterize the regions of tissue damage following cryoinjury, Green Fluorescent Protein (GFP) transfected tissues were cryoinjured using a cryoprobe circulating liquid nitrogen. The long-term fluorescent yield of transfected tissues was observed in a controlled environment to determine the tissue's fluorescent response to cryoinjury. Other phenomena that impact fluorescent intensity were controlled and/or observed to eliminate these effects as the source of changing fluorescent intensity. It was observed that following cryoinjury, GFP fluorescence within tissues decays with a trend that follows Fick's second law of diffusion, suggesting that cryoinjury does not directly affect fluorescence, but allows the onset of GFP diffusion through and out of cryoinjured regions. Additional studies designed to account for the movement of all GFP within a closed system support this conclusion. It was determined that GFP-transfected tissues can effectively indicate cryoinjury, provided that conditions are favorable to diffusion.

Emerging techniques that combine cryosurgery with laser heating need accurate methods to simulate the thermal response of a cryogenic tissue to optical irradiation. Light transport in tissue has been studied in great depth, and various computer programs and models currently exist that simulate light transport in simple systems. Light transport in tissues that undergo large changes in temperature, such as those encountered with laser-irradiated cryogenic tissues, cannot be accurately modeled with traditional

methods, as those methods rely on simple geometries and optical properties which are constant with respect to temperature. A computer program and the supporting algorithms was developed which allows for the simulation of light transport in arbitrarily-shaped tissues which have temperature-dependent thermal and optical properties. The program first determines the optical distribution/deposition within the tissue, using a Monte Carlo photon heating simulation. The volumetric heating data is then used in determining heat transfer within the system. Optical properties based on the new thermal profile are interpolated and the optical distribution is repeated using these updated optical properties. This process repeats itself as necessary for the duration of the simulation. The simulation results compare favorably to established laser-tissue simulations, and to fundamental laws, validating the accuracy of the simulation outputs. The simulation can accurately predict the thermal response of a geometrically-complicated system to optical irradiation, including systems that undergo large changes in temperature and thus large changes in optical and thermal properties.

TABLE OF CONTENTS

Acknowledgements.....	iv
Table of Contents.....	x
List of Figures	xiii
List of Tables.	xv
List of Equations.....	xvi
Chapter 1 Introduction	1
Chapter 2 Laser-Assisted Cryosurgery.....	6
2.1 Introduction.....	6
2.2 Materials and Methods.....	6
2.3 Results and Conclusion.....	8
Chapter 3 Green Fluorescent Protein as an Indicator of Cryoinjury in Tissues.....	10
3.1 Abstract	10
3.2 Introduction.....	11
3.3 Materials and Methods.....	14
3.4 Results	26
3.5 Discussion	32
3.6 Conclusion	34

Chapter 4	Monte Carlo Method for Photon Heating Using Temperature-Dependent Optical Properties	36
4.1	Abstract	36
4.2	Introduction.....	37
4.3	Description of Method	39
4.4	Validation	45
4.5	Heat Transfer.....	49
4.6	Representative Simulation	54
4.7	Discussion and Conclusion	55
Chapter 5	Discussion and Conclusion	58
5.1	Discussion.....	58
5.2	Conclusion	63
	Bibliography.....	67
Appendix A	VOIDSim User Manual	71
A.1	Preface.....	71
A.2	VOIDSim.....	71
A.3	System Requirements and Recommendations	72
A.4	Installation/Uninstallation of VOIDSim	73

A.5	User Interface.....	74
A.6	Additional Help.....	99
A.7	Glossary.....	100

LIST OF FIGURES

Figure 1.1 2

Figure 2.1 7

Figure 2.2 9

Figure 3.1 14

Figure 3.2 18

Figure 3.3 20

Figure 3.4 23

Figure 3.5 27

Figure 3.6 28

Figure 3.7 30

Figure 3.8 31

Figure 4.1 39

Figure 4.2 41

Figure 4.3 49

Figure 4.4 50

Figure 4.5 51

Figure 4.6 52

Figure 4.7 54

Figure 4.8 55

Figure 5.1 59

Figure 5.2	60
Figure 5.3	61

LIST OF TABLES

Table 4.1 – Semi-infinite slab reflectance.....	46
Table 4.2 - Thin-slab reflectance and transmittance	46
Table 4.3 - Multiple layers reflection and transmission	47
Table 4.4 - Optical absorption coefficient of silicon at 1180 nm.....	47
Table 4.5 - Constant properties of silicon.....	48
Table 4.6 - Thermal properties of water in two phases	53

LIST OF EQUATIONS

Equation 3.1 – Adjusted Luminance	21
Equation 3.2 – Fick’s Second Law of Diffusion.....	23
Equation 3.3 - Characteristic Length of Diffusion	24
Equation 4.1 - Beer-Lambert law for absorption	48
Equation 4.2 - Lumped-capacitance ODE	49

CHAPTER 1 INTRODUCTION

Cryosurgery can be described as the surgical application of cold. Most often this surgical application of cold intends to destroy a targeted tissue, through cell rupture or dehydration [3]. It has been demonstrated to be an effective treatment in the treatment of viral warts, seborrheic keratoses, molluscum contagiosum, spider angiomas and digital myxoid cysts [4]. In addition to topical applications it can be used within the body cavity, and is often used in tumor destruction (such as kidney or prostate cancer) via percutaneous surgery. Cryosurgery is an attractive alternative to more traditional surgeries (i.e. open-cavity surgery) because it is simple, less-invasive, inexpensive, and safe [5].

Since the mid 1850's cryosurgery has been demonstrated to be effective in treating a variety of tissues. Campbell White first used liquefied air for medical use in 1899. In 1913 Dr. Irving Cooper invented the liquid nitrogen cryoprobe, which greatly increased the potential applications for cryosurgery within the body. Cryogenic sprays were introduced in the mid 1960's, allowing for doctor's office use [5]. While the application of cold (removal of heat) can be precisely administered, the diffusion of heat is not as easily controlled. The imprecise nature of cryosurgery limited its utility until the 1990's. In the 1990's new techniques, including monitoring ice propagation during cryosurgery and active warming [6], were developed that greatly reduced the extent of collateral damage.

The imprecise nature of cryosurgery leads to difficulty in ascertaining the extents of cryoinjury during cryosurgery, which in turn may lead to either incomplete target-tissue destruction or overcompensation and significant collateral damage (Figure 1.1). While improvements in cryosurgery have lessened this effect, there exists need to further refine cryosurgery. Currently cryosurgery is often not a viable candidate for tumor treatment due to the presence of sensitive nerves, tissues, or organs in the area adjacent to the tumor.

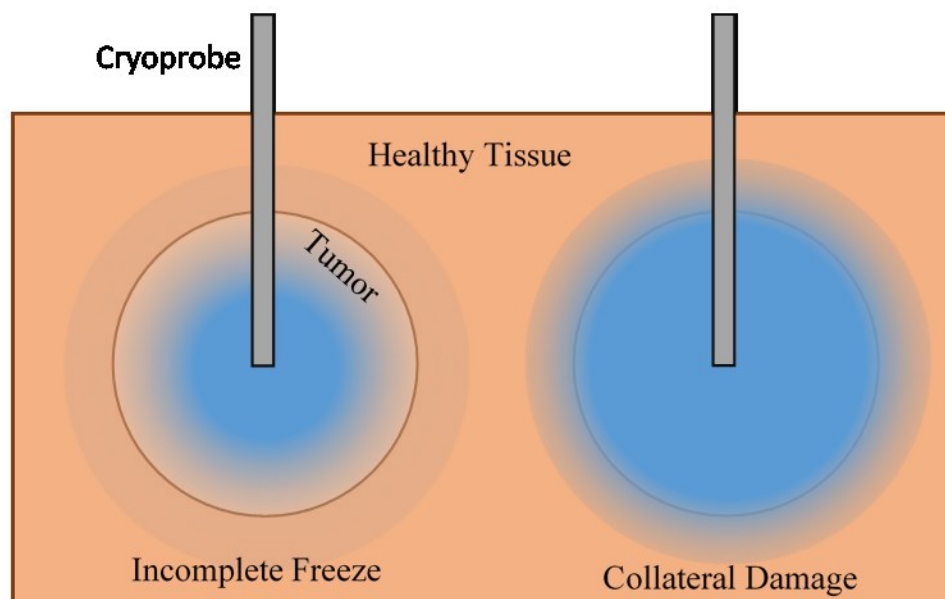


Figure 1.1 - Cryosurgery

The current practice of percutaneous cryosurgery involves positioning a single or multiple cryoprobes/cryoneedles within a targeted tumor. Liquid nitrogen, or another cryogen, is circulated within the needle. The uninsulated cryoneedle tip then freezes the surrounding tissue, and the ice formation expands from the needle tip. The positioning of

the needle, and the monitoring of the ice propagation is often monitored using ultrasound imaging.

Part of the challenge to cryosurgery is in preventing damage to surrounding, healthy tissues (Figure 1.1) while ensuring complete tumor destruction. Chapter 2 outlines research completed on a technique to actively heat surrounding tissues using optical heating. Dubbed “Laser-Assisted-Cryosurgery” this technique applies laser heating to counteract ice propagation, thus preserving the viability of protected tissues. This research consists of physically exposing mouse hepatic tissue to a cryogenic process while warming a part of that tissue with laser heating. The viability of the tissue following these procedure is assessed to determine the efficacy of this method.

To assess the viability of tissues following cryosurgery, multiple biopsies, or toxic chemical tracers are often introduced into a tissue. These procedures require large amounts of time and effort and cannot be done *in situ*, while other procedures introduce toxic or phototoxic chemicals into the tissue which can cause cellular death. Current tissue viability procedures present a significant hindrance to expedited cryosurgery research. Chapter 3 presents research completed on a visual method to ascertain the regions of cryoinjury in a tissue following cryoinsult, without introducing chemical tracers or requiring biopsies. The method utilizes Green Fluorescent Protein (GFP) transfected tissues to visualize cryoinjury. The method correlates tissue fluorescence to cryoinjury, allowing a researcher to quickly visualize the regions of thermal destruction. To

demonstrate this correlation a tissue is continuously visualized and monitored for changes in fluorescence, from cryoinjury until complete loss of viability. These results are analyzed to determine the cause of fluorescence loss while accounting for known phenomena that affect fluorescence.

Especially in the age of computers, numerical simulation of physical systems is especially attractive to a researcher as it can save valuable time and resources. Many simulations currently exist that are able to model laser-tissue interactions, however all of them are limited in the geometries they can model. Furthermore Chapter 4 establishes the need for these models to include temperature-dependent optical properties, which no existing simulation can presently do. Chapter 4 introduces a numerical method, and its associated computer program, that was developed to accurately model light transport within cryogenic tissues and their subsequent thermal response to the light distribution. The software dynamically couples light propagation to heat transfer to incorporate temperature-sensitive thermal and optical properties for a simulation with unparalleled accuracy in results for certain conditions. The simulation is validated against existing numerical results, and against fundamental laws governing variable optical properties.

Taken together, this dissertation provides tools and techniques to further enhance cryosurgical procedures, and cryosurgery research. As the efficacy of cryosurgery is increased, and the negative side-effects are decreased, cryosurgery can find applications where it previously was not viable, providing a low-cost, more effective option for treating

an expanding variety of ailments. The knowledge presented here is not limited to cryosurgical applications, as the research presented in Chapter 4 can revolutionize the way any laser-tissue interactions are simulated.

CHAPTER 2 LASER-ASSISTED CRYOSURGERY

Laser-Assisted Cryosurgery (LAC) is a concept conceived, developed, and tested principally by Lorenzo Martínez-Suástegui with collaboration from additional researchers, including this author. The full contents of the publication resulting from that work are found in [2].

2.1 Introduction

In cryosurgery a main challenge is to control the expansion of the freezing front of the ice ball propagating from the cryoprobe tip. LAC involves counteracting the freezing front induced in cryosurgery using laser heating. Sensitive regions of tissue are shielded from the ice-propagation through laser warming while still permitting the tumor region to be completely frozen and destroyed. As the freezing front approaches a sensitive region of tissue, laser heating is selectively switched on and off to warm the protected region.

2.2 Materials and Methods

A 2.6 x 5 x 10 mm slice of hepatic tissue was excised from a GFP-transfected mouse. Green Fluorescent Protein (GFP) transfected tissue was used to facilitate the visualization of the thermally damaged regions of tissue. The tissue was placed in a holder where one side was brought into contact with a cryoprobe. The cryoprobe circulated liquid nitrogen, and the temperature of its tip was monitored with a thermocouple and

found to be constant at $-196\text{ }^{\circ}\text{C}$. The other side of the tissue was exposed to pulsed laser irradiation at 1320 nm , as seen in Figure 2.1.

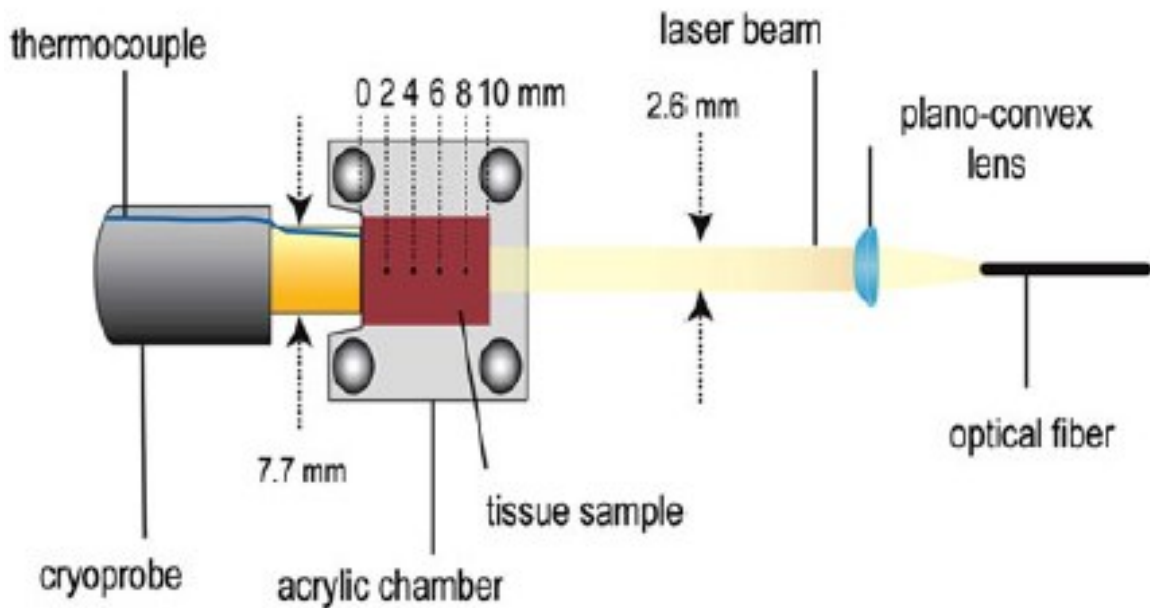


Figure 2.1 - LAC Setup. Image from [2].

Temperature of the tissue was monitored in real-time with an array of thermocouples placed every 2 mm within the tissue, as well as the aforementioned thermocouple attached to the cryoprobe. At the start of the experiment, the liquid nitrogen circulation within the cryoprobe is turned on, and the probe quickly cools to the constant $-196\text{ }^{\circ}\text{C}$. As heat is removed from the adjacent tissue, the tissue becomes frozen, starting from the left side (Figure 2.1) and moving toward the right. As the freezing front approaches the right side of the tissue, laser heating is switched on and off as necessary to prevent the final 2 mm of tissue from freezing, simultaneously taking care to not elevate the tissue temperature to a point detrimental to tissue health.

After treatment, the tissue was removed from the holder, and analyzed for tissue viability using reverse transcriptase polymerase chain reaction (RT-PCR) analysis.

2.3 Results and Conclusion

It was found that counteracting the freezing front propagation with laser heating was successful in preserving the viability of the region targeted for thermal protection, while ensuring the destruction of the remaining tissue, with a small zone between the two regions. Furthermore it was shown that the location of the freezing front can be halted and held at a constant position using this procedure. LAC can be utilized to increase the selectivity of tissue targeted for destruction, thereby enhancing cryosurgery.

To visualize the regions of tissue destruction/survival, GFP fluorescent images of the tissue were taken and are shown in Figure 2.2. The necrotic regions of tissue no longer fluoresce as brightly as they once did while the fluorescence of the protected region retains its original brightness. While these regions correlate to the tissue viability ascertained using RT-PCR analysis suggesting a correlation between viability and fluorescence, the mechanism of lost fluorescence in the tissue was unknown. This mechanism of lost fluorescence was the major motivation driving the research presented in Chapter 3.

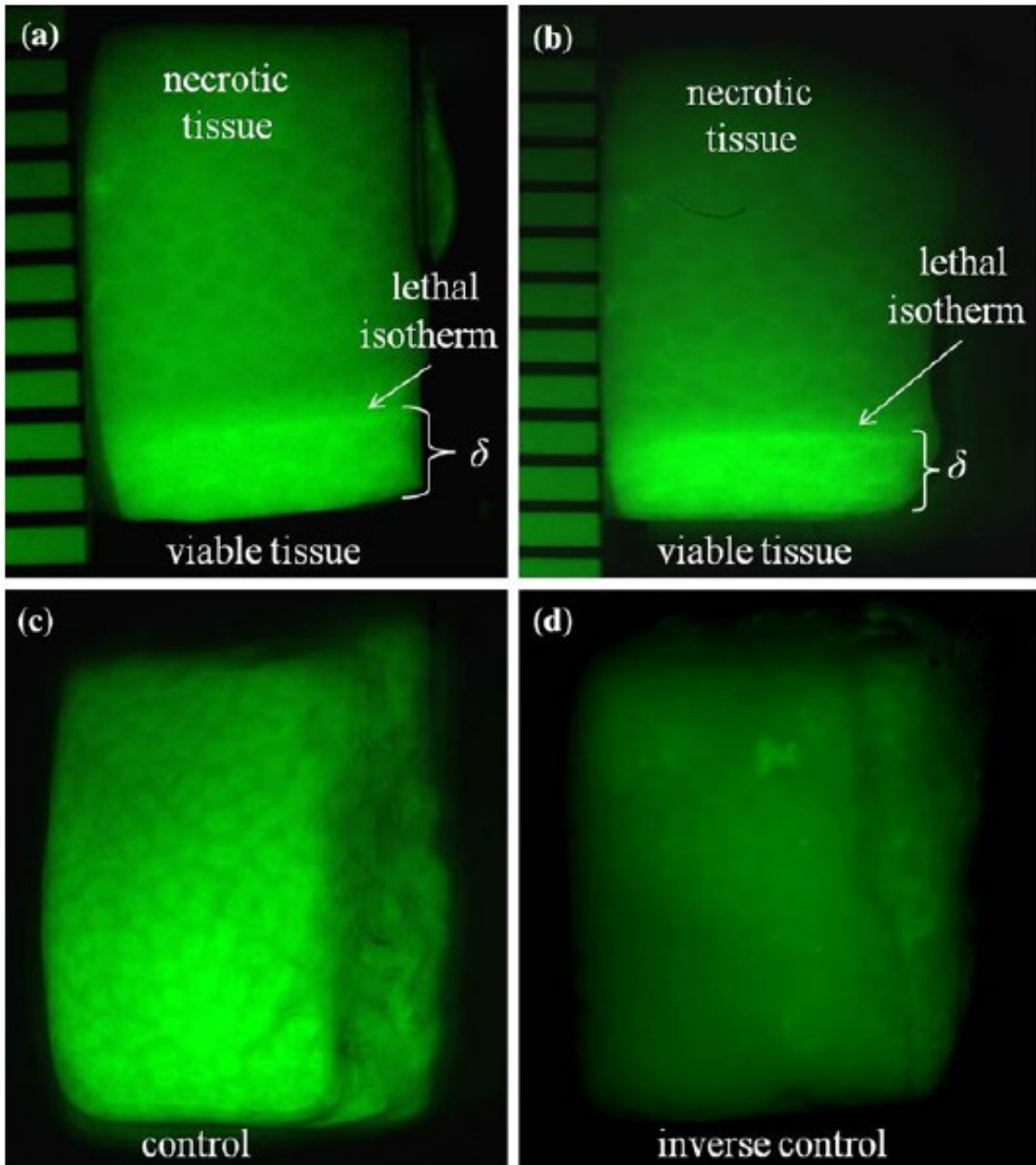


Figure 2.2 - GFP fluorescence contrast, correlating to cellular viability. Image from [2].

CHAPTER 3 GREEN FLUORESCENT PROTEIN AS AN INDICATOR OF CRYOINJURY IN TISSUES

The whole of Chapter 3 is a reproduction of “Green Fluorescent Protein as an Indicator of Cryoinjury in Tissues”, published in *Annals of Biomedical Engineering* in December 2013, Volume 41, Issue 12, pages 2676 – 2686 [1]. It is reproduced here with kind permission from Springer Science and Business Media.

3.1 Abstract

The fluorescence intensity of Green Fluorescent Protein (GFP) has previously been demonstrated to be an accurate indicator of cellular viability following cryoinsult in individual GFP-transfected cells. In an attempt to ascertain whether GFP fluorescence intensity may also be used as a viability indicator following cryogenic insults in whole tissues, this study examines the transient fluorescence intensity of GFP-transfected mouse hepatic tissue *ex vivo* following cryoinsult. The observed trends are compared with diffusion-based models. It was observed that the fluorescence intensity of the exposed tissues exhibited slow exponential decay, while the solution in which the tissues were placed inversely gained fluorescence. This slow decay (approx. 3 hours) is in contrast to the rapidly diminished fluorescence intensity (seconds) seen in GFP-cell cultures following cryoinsult. These trends suggest that mass diffusion of GFP in the interstitial space, and ultimately into the surrounding medium, is the primary mechanism which determines the fluorescence loss in cryoinjured tissues. These results suggest GFP-transfected tissues may be effectively used as indicators of cryoinjury, and hence viability, following

hypothermal insult provided that a sufficiently long incubation is held before observation. It was found that a meaningful observation (15% reduction in fluorescence) could be made three hours subsequent to cryoinjury for the tissues used in this study.

3.2 Introduction

Cryosurgery—the precise application of cryogenic temperatures—is often used to selectively devitalize cancerous or precancerous tumors, arresting its propagation through healthy tissue. These low temperatures serve to rupture the plasma cell membranes, or to dehydrate the cells as to render their vitality compromised. To determine the success of a cryosurgical protocol, it is of critical importance that the tissues cryogenically treated, as well as the surrounding tissues, be evaluated for their viability. Current viability protocols require the tissue to be excised from the treatment site and examined *in vitro* [7, 8]. These procedures are invasive and provide only information traceable to the moment in time when the biopsy was obtained. Non-invasive viability assays can be utilized to determine cellular viability, but require the addition of chemical tracers (which are often toxic or phototoxic) to the living tissue [9]. While viability can be determined optically without tracers, this is done on a cell-to-cell basis [10], and assessing the viability of a whole tissue would not be feasible using those methods.

Green Fluorescent Protein (GFP) is a protein derived from jellyfish which can be and has been transposed into the genome of a myriad of organisms. It has the effect of

causing transfected tissues to fluoresce green when illuminated with blue light, and has recently found use as a viability assay in cell cultures [11]. GFP has the advantage over other viability assays in that it can be examined *in situ*, and can also be continuously monitored to examine the transient viability of the cells using optical imaging, thereby making it an ideal indicator of animal tissue viability in research protocols.

The GFP molecule has a tight cylindrical barrel shape, which protects it from a moderate range of thermal trauma [12], however, at sufficiently elevated temperatures (>50 °C) its structure becomes "unwound", it is compromised (irreversibly denatured) and exhibits loss of fluorescence [13]. In contrast, after exposing GFP cells to cryogenic temperatures (liquid nitrogen: -196°C), they appear to remain stable and exhibit only a slightly reduced quantum fluorescent yield [14, 15]. Therefore, while GFP-transfected tissue exhibits immediate loss of fluorescence following hyperthermal insults, hypothermal insults have no such immediate effect. In fact, in preliminary trials using GFP as an indicator of viability in whole tissues, it was observed that there is a delayed response on the order of several hours to changes in fluorescence in cryoinjured tissues [2]. In addition to temperature, GFP fluorescence also exhibits sensitivity to the pH of its environment. However, while the fluorescent yield drops off in very acidic or basic solutions, there is a relatively wide range of pH values for which fluorescence is stable [13, 16].

This tissue-based study are in contrast with single cell studies, which report immediate fluorescence change following both hyperthermal and hypothermal insults [11]. Furthermore, in the latter study focused on cell cultures, it was implied that the loss of cell fluorescence following cryoinsult corresponds with the physical loss of GFP from inside a GFP-transfected cell, however, it was not demonstrated conclusively that this was the only driver contributing to fluorescence loss, nor was the transient fluorescence intensity decay following cryoinsult reported. This opened an interesting quandary as it is also plausible, in principle, that the viability of cells transfected with the GFP vector is also linked to the relative amount of expressed fluorescence, with the most brightly fluorescing cells being viable, and apoptotic or necrotic cells exhibiting diminished fluorescence [17].

This work aims to observe the time-dependent nature of GFP fluorescence to identify the mechanism that drives fluorescence loss after hypothermal insults. For this purpose, it is hypothesized that there is a relationship between the fluorescence of a GFP-transfected tissue post-cryogenic insult and the rate of diffusion of GFP from the compromised tissue into the surrounding tissue or incubation medium. To prove this hypothesis, the known phenomena which affect the fluorescence of GFP (i.e., pH, temperature, excitation light intensity and excitation duration) are maintained within ranges known not to affect GFP fluorescence yield. The transient fluorescence of a cryogenically-treated tissue is then compared to mass diffusion models to determine its correlation (or lack thereof). Finally, the fluorescence of the incubation medium is

compared to the total fluorescence of the tissue to establish a balance between tissue and incubation medium fluorescence gain/loss.

3.3 Materials and Methods

3.3.1 GFP Tissue Harvesting and Sample Preparation

The strain of GFP used in this study is the enhanced GFP which has an electromagnetic radiation absorption (excitation) peak at 488 nm (blue light), and an emission peak at 509 nm (green light) (Figure 3.1).

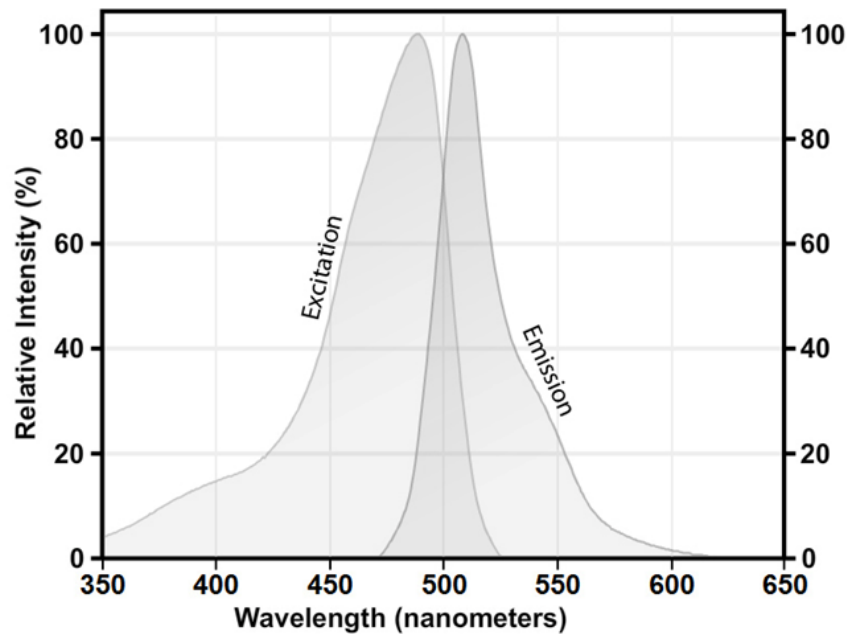


Figure 3.1 - GFP excitation and emission curves. Adapted from [18].

According to protocols A-20080013 and A-20080019, approved by the UCR Institutional Animal Care and Use Committee (IACUC), all GFP-transfected tissues used in this study were harvested from the hepatic tissue of GFP-transfected mice. This specific tissue was chosen due to its large size, ease of extraction and similar thermal properties

compared to other available organs [2]. The specific GFP vector transcription used, C57BL/6-tg(UBC-GFP)30Scha/J, universally expresses GFP in mouse tissue under the human ubiquitin C (UBC) promoter [19]. This strain of GFP was used as it has relatively little overlap in its excitation and emission curves (only between 470 and 530 nm), thus the excitation source light may be completely isolated from captured emission light from the tissue to eliminate all crossover illumination.

After the mice were euthanized via CO₂ asphyxiation, the liver was excised and cut into squares of 6 x 6 mm, and left at its native thickness of approximately (but not uniformly, exactly) 4.4 mm. The thickness of the samples varied spatially by up to approximately 20% from their mean value, as determined visually. These dimensions were chosen as they were similar in size to previous GFP-tissue studies performed in this laboratory [2]. Following excision and trimming, all samples were immersed together in 50 mL of isotonic Phosphate Buffered Saline (PBS) solution (pH 7.4) to prevent tissue damage due to cellular dehydration. The PBS also served to maintain the pH level without significant change. Samples remained in this holding vessel for approximately two minutes to allow for experimental preparation time.

Control samples were removed from the holding vessel and placed in an isolated 34 mm cylindrical vessel and covered with 5 mL of fresh PBS. The samples slated for cryoinjury were removed from the holding vessel, and one side was exposed for one minute to a cryoprobe cooled by circulating liquid nitrogen at -196°C. This exposure time

was long enough to ensure that the entire sample was uniformly cooled to a temperature of -150°C or lower as measured by a 0.2mm-diameter hypodermic thermocouple inserted in to the sample's center, ensuring complete cellular necrosis. Following the cryoprobe contact, cryoinjured samples were placed in fresh PBS (identical to control tissues) at room temperature (23°C), thawing in a few seconds. Nothing was placed over the sample/PBS as to keep the optical path clear. Both the cryoinjured samples and control samples were then isolated from all light to prevent photobleaching. Ten tissue samples were used in the experiments, with five as control tissues (no thermal damage) and the remainder as cryogenically injured tissues (necrotic). In addition, one sample served as an inverse control, where all GFP within the tissue was irreversibly denatured through immersing the sample in water at 100°C for five minutes. Also, a set of four samples were prepared for qualitative visual analysis, consisting of two tissue samples prepared in the same manner as the control/cryogenic treatments described above; one sample cryogenically treated through submersion in liquid nitrogen for five minutes; and one sample boiled in water for five minutes.

3.3.2 Fluorescent Image Acquisition

A custom fluorescence microscope was constructed to measure the fluorescence intensity of the GFP-transfected tissue as a function of time. A brief description of the experimental apparatus is as follows:

When the sample is to be illuminated (fluorescently excited), a mechanical shutter blocking a broadband light source (Fiber Lite® MI-150 utilizing an EKE 21 V 150 W halogen projector lamp routed via stock fiber optics) opens (Figure 3.2(1)), allowing light to proceed through focusing optics and a low-pass excitation filter (Thorlabs, model FES0500). The mechanical shutter is used to limit exposure and thus prevent photobleach of the GFP within the tissue. After the light passes through the shutter and excitation filter, the light reflects off a dichroic filter (Thorlabs, model DMLP505, Figure 3.2(2)) whose surface is positioned 45° to the incoming light. This filter selectively transmits or reflects the light (high-pass, low-reflect), further narrowing the bandwidth of excitation light. The reflected light illuminates the tissue at approximately 215 W/m² (Figure 3.2(3)) where it is both in part reflected and absorbed. A portion of the absorbed light excites the GFP within the tissue, which reemits this absorbed light at a longer wavelength. The light which is reemitted in the upwards direction passes through the dichroic filter again at an angle of incidence of 45° (high-pass, low-reflect), followed by a band-pass emission filter (Thorlabs, model FB550-40), that isolates pure GFP fluorescence from reflected illumination light. This isolated fluorescence then passes through the camera's RGB Bayer-pattern filter (designed to record wavelength information) and then is collected by the CCD's (Sony IXC282AQ Super HAD CCD) capacitive bins (Figure 3.2(4)). Note that the optical setup could be achieved using a modified optical path. For example, the dichroic could be used without the excitation filter to allow for greater light excitation, and the

excitation light may include all wavelengths shorter than the pass-wavelength of the excitation filter, if so desired.

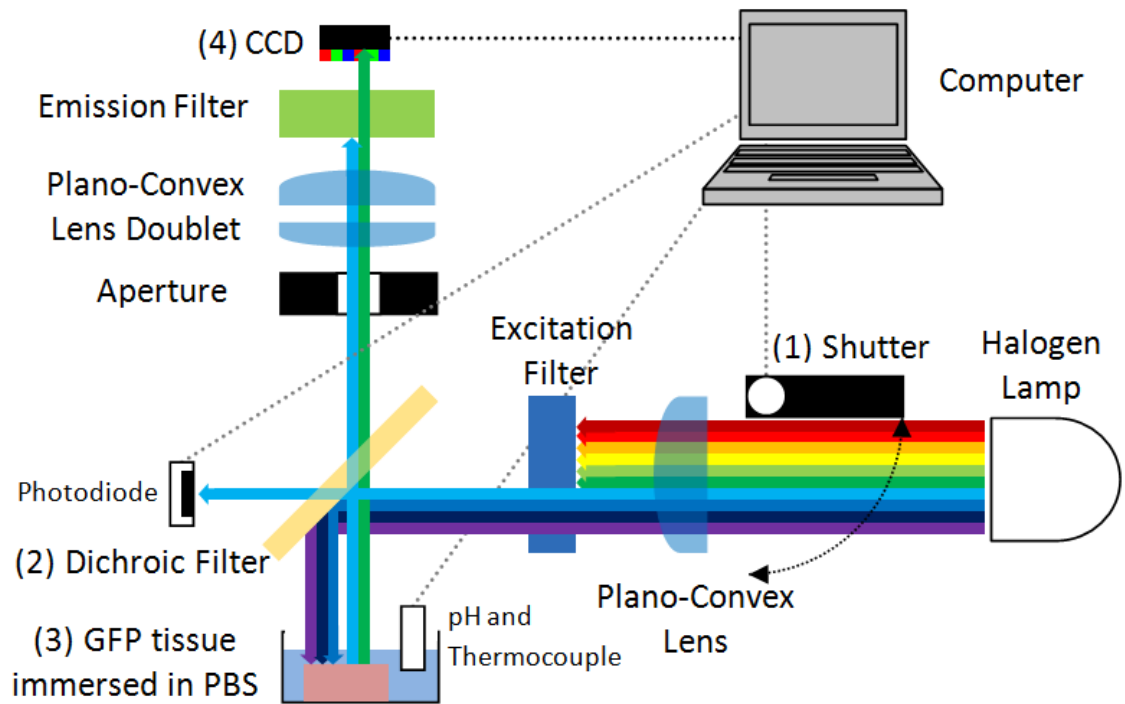


Figure 3.2 – Automated isolation and collection of GFP fluorescence

The CCD begins photon capture after the mechanical shutter opens. The electronic shutter stays open long enough for the CCD to collect enough light to produce an image, but not beyond the time in which any particular capacitive bin might saturate. After this predetermined length of exposure (directly proportional to the illumination intensity), both the CCD's electronic shutter and the mechanical shutter close. As the entire system is isolated from ambient light, this leaves the sample in complete darkness until the next image is to be acquired, negating the possibility of photobleaching. This computer-controlled system exposes and images a single sample for five seconds once every three minutes. This imaging process was allowed to proceed over the course of several hours,

until the tissue fluorescence reached a steady value (6-12 hours). All imaging components were permitted to reach their steady state temperature before imaging commenced. Electronic noise inherent in the sensor was averaged out over space and time, that is, the brightness of the image was taken as a regional average (described below), and smoothed among subsequent images.

3.3.3 Data Processing

It was observed that while the samples generally exhibited a decrease in fluorescence over the acquisition period, the PBS in which the samples were placed steadily increased in fluorescence. Both the tissue and PBS fluorescence intensities were measured by acquiring CCD images from two different regions. One region of the image contains the GFP tissue (along with the PBS on top of the tissue) and the other region of interest is to the side of the tissue sample where only PBS was imaged. Each image in the sequence had the same field of view (neither the sample nor imager were moving), and as such a constant subset of the image was determined spatially and applied to all subsequent images. These regions were determined as a maximized region (greater than 80% of the surface area) consisting of only tissue/PBS which provided no overlap between the two regions, as shown in Figure 3.3.

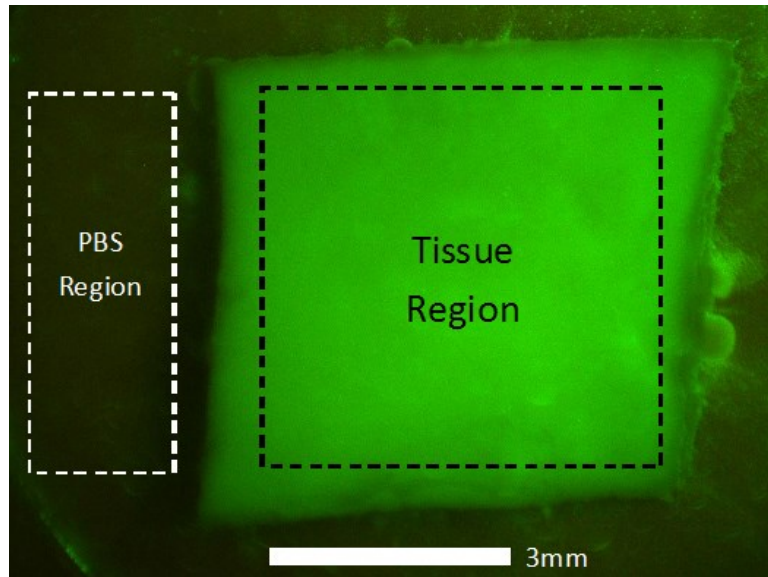


Figure 3.3 - Regions of GFP fluorescence image analysis

Using the known depth of the PBS over the sample (typically 1.3 mm), and the depth of the PBS to the side of the sample (typically 5.7 mm), the fluorescent contribution of the PBS to the tissue region may be subtracted from the fluorescence of the tissue at every time step, resulting in a fluorescent value which is independent of the fluorescence of the surrounding fluid. A separate photodiode recorded the relative illumination intensity of the sample (not wavelength), to ensure consistent sample excitation. Simultaneously, a calibrated type-K thermocouple and calibrated pH probe recorded the temperature and pH of the solution. After each five second exposure, the CCD sensor data was sent to a computer where it was compiled into a JPEG image of the sample. The mechanical shutter, image acquisition, pH data recording, photodiode data recording, and data storage were all managed autonomously by a custom LabVIEW® program controlling and getting data from DAQ controllers (National Instruments). pH and image

acquisition were done with a pH sensor (Sensorx[®] S100C) and a scientific grade camera (Progres[®] C5), respectively.

After the sequence of images was collected, a custom MATLAB[®] program analyzed the images from the two stationary regions previously described (tissue, and surrounding PBS) to determine their relative brightness (luminosity), and a correction factor was applied for each image to account for PBS fluorescence affecting the GFP fluorescence. This correction factor was calculated as the relative brightness of the incubation fluid in the region without tissue, versus the region containing tissue. Furthermore, the data from the photodiode which measured the source light intensity was included for an additional correction factor to rectify any differences in the illumination source.

The basic algorithm of the code included applying the user-defined crops to each image region. The digital-filter was then applied by deleting the blue-channel data from the image. The average spatial luminances of the tissue crop and PBS crop were determined ($AvIm$). Finally the adjusted luminance of the tissue crop ($AdIm$) was obtained by subtraction of the product of the PBS luminance ($AvPBS$) with the determined percentage of PBS depth above the tissue ($PerOver$) (typically 23%) from the average luminance, as shown in the following equation. This was repeated for all images in the sequence, as denoted by the subscript in Equation 3.1.

$$AdIm_i = AvIm_i - (PerOver * AvPBS_i)$$

Equation 3.1 – Adjusted Luminance

The output from the MATLAB® image analysis was a matrix giving the raw and corrected tissue luminance for each time step. As it was assumed that GFP fluoresces most brightly in healthy, viable tissue, and that the tissue was most healthy/viable immediately after harvest, the first time step was defined as 100% luminance, and all the data was normalized to that time step. When plotted, this gives the normalized luminance of the tissue versus time. It is also noted that the CCD used was tested for its linear response to illumination levels, to ensure that relative fluorescence levels were directly proportional to their relative CCD values.

The data processing workflow for image acquisition is displayed in Figure 3.4.

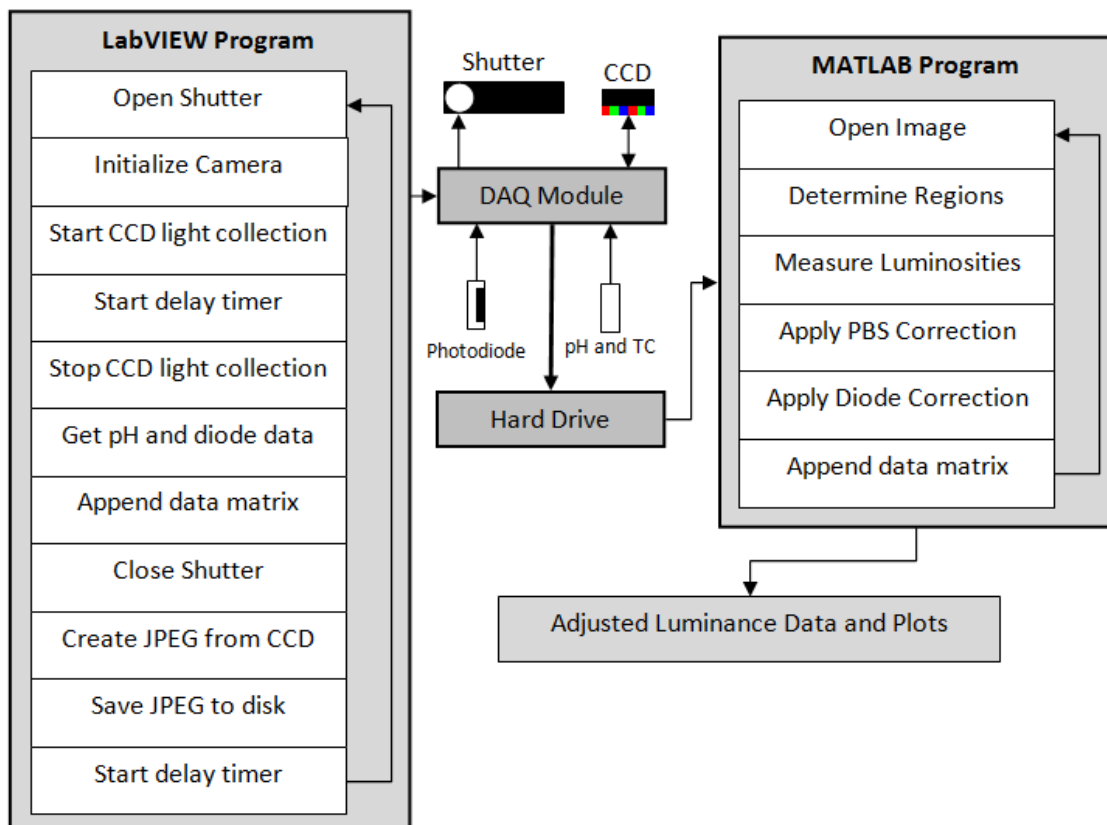


Figure 3.4 – Automated data acquisition and processing flow

3.3.4 Finite Element Method (FEM) Modeling

To test the hypothesis of diffusion driving the transient nature of the fluorescence, a finite element method model was created using COMSOL® simulation software. The intention of the model was to examine if transient diffusion was the only physical phenomenon responsible for the fluorescent intensity loss of the treated tissue samples. The model involved three-dimensional diffusion in a constant-temperature environment. The governing equation used by the software to evaluate the concentration gradients is based on Fick's second law,

$$\delta_{ts} \frac{\partial c}{\partial t} + \nabla \cdot (-D \nabla c) = R$$

Equation 3.2 – Fick's Second Law of Diffusion

where D is the diffusion coefficient for GFP in extracellular-matrix, c is the concentration, R (set to zero) is the reaction rate, and δ is the time-scale coefficient (set to 1, to reflect actual time). The approximations used assume dilute aqueous solutions and, while the tissue is not an aqueous solution, the fluid content of the tissue is sufficiently high that the approximation is valid. Also note that D for GFP in extracellular-matrix is used in our simulations with a value of $5.6E-11 \text{ m}^2/\text{s}$ [20-22], rather than the diffusion coefficient of GFP in tissue because the simulation is only meant as an order-of-magnitude comparison to the observed loss of fluorescence. Also, while the diffusion coefficient of GFP within the nucleus or cytosol is reported in the literature (e.g. [23]), the value for GFP in mouse hepatic tissue is not readily available. The size of the simulated tissue matched that of the

experimental tissue (6 x 6 x 4.4 mm), and the initial normalized concentration (c) of the sample was set to 1 (100%). All boundary conditions of the model were approximated as a constant concentration (c) of zero, as it is assumed that the surrounding fluid contains no GFP and that the far-removed boundaries remain at that concentration as time progresses. This approximation is valid as a large fluid-to-tissue volume ratio (32:1) was used in the experiments.

As an order of magnitude analysis, the characteristic length of diffusion is useful:

$$L_D = \sqrt{4Dt}$$

Equation 3.3 - Characteristic Length of Diffusion

where L_D is the diffusion length, D is the diffusion coefficient, and t is a characteristic time. This will be used to explain the differences between single cell GFP viability experiments, and experiments using bulk tissue samples.

As visualization of the COMSOL® model would have to match the optical properties of the experimental tissue, one further, major, approximation was made. The model was assumed to have no diffusion across the bottom surface. In reality there would be no diffusion across the bottom surface, as it was not exposed to the surrounding PBS (in contact with bottom surface of Petri dish), but the top surface was exposed to PBS and would naturally have some diffusion. The depth of PBS above the tissue in the experiments was minimized (approx. 1.3 mm) so as to minimize diffusion in that direction, while still keeping the sample hydrated. As the top and bottom surfaces were more-or-less boundaries to diffusion, and seeing that the optical depth of the tissue was unknown,

the computational model was collapsed to be a two-dimensional model (with a 6x6 mm domain) by taking the average fluorescence at all depths (z-direction). All boundary conditions and coefficients used were identical to the 3D model.

3.3.5 *GFP Conservation*

GFP originally within the tissue was traced from its origin to its final position with the objective to assess the total fluorescence of the entire system (PBS and tissue) for all time steps. The goal was to determine if fluorescence intensity loss in the tissue was simply due to diffusion to the surrounding media or if GFP was destroyed or denatured during the procedure. The challenge to this analysis was in that not all fluorescence in the tissue is available to excitation or collection of emission at all times, due to a finite optical penetration depth of the tissue. To examine all fluorescence potential of the tissue, the tissue was dissociated into a suspension of individual cells. This was done with three sets of six tissue samples (18 tissue samples). Each set had three samples dedicated to cryoinjury, and three to control.

In the dissociation procedure, tissue samples were treated with identical thermal insults as in the traditional experiment, however, after incubating in PBS, the sample was removed to a new volume of PBS mixed with collagenase enzyme (to target only collagen peptide bonds, ignoring all other structures (i.e. GFP) [24]), for extracellular matrix dissolution at a concentration of 100 units/mL. The sample was then permitted to dissociate over the next 24 hours, after which fluorescence of the resulting mixture was

examined. As the intention was to examine the average fluorescence of the entire system, cellular integrity did not matter at this point, only GFP integrity. The original incubation PBS was retained for fluorescent analysis, independent of the fluorescence of the dissociated tissue.

As each time-step required an entire tissue sample to be dissociated, samples were only obtained at one, three, and six hour's duration, due to limited resources. While this distribution is not ideal for determining the rapid response of GFP fluorescence, it proved to be sufficient in demonstrating the overall trends in fluorescence. Three complete data sets were obtained and averaged using this procedure, for a total of nine samples for the control, and nine for the cryoinjured sample.

3.4 Results

3.4.1 Constant pH/Illumination/Temperature

Figure 3.5 shows the transient pH profile of PBS for a representative experiment. As it has been established that the fluorescent output of GFP is stable within a range of pH from 6 to 10 [13, 16], it is understood that the observed change in pH will not have any impact of the fluorescent yield of the GFP.

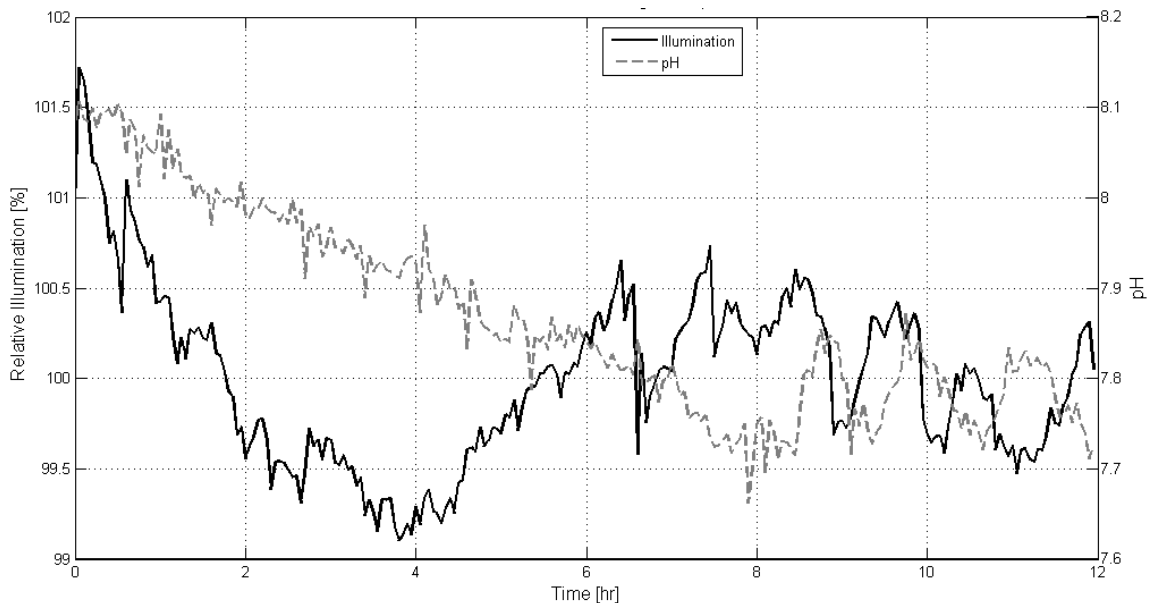


Figure 3.5 - Variation of pH and illumination intensity with time

The transient level of excitation light for a representative experiment also shows minimal variability not exceeding 5% of the average value (Figure 3.5), however, the fluorescent output of the sample is highly dependent on the illumination intensity, and should be compensated for. To achieve this compensation, each time step was normalized to the measured excitation level for that particular time step.

Finally, the temperature of the system was determined at every time step, and never varied more than $\pm 2^\circ\text{C}$ from a mean value of 23°C . This minimal variability has negligible influence over GFP fluorescence [15].

3.4.2 Optical Results

Figure 3.6 is subdivided into 4 quadrants (A-D), all of them showing the fluorescent images of 4 samples immediately after thermal insults (quadrants A and C) and 20 hours after incubation (quadrants B and D). The top two quadrants (A and B) and bottom two

(C and D) represent the same set of four samples, only with crossover between excitation illumination and fluorescent emission (top) and filtered pure fluorescence (bottom). The top left image of each quadrant is the control sample; the top right corresponds to the inverse control, and the bottom images to the two cryoinjured samples. The bottom left corresponding to the sample exposed to the cryoprobe for 1 minute, the bottom right to that immersed in liquid nitrogen for 5 minutes. These results are only presented here to provide a conceptual illustration of the results, and these images were not analyzed for numerical data extraction.

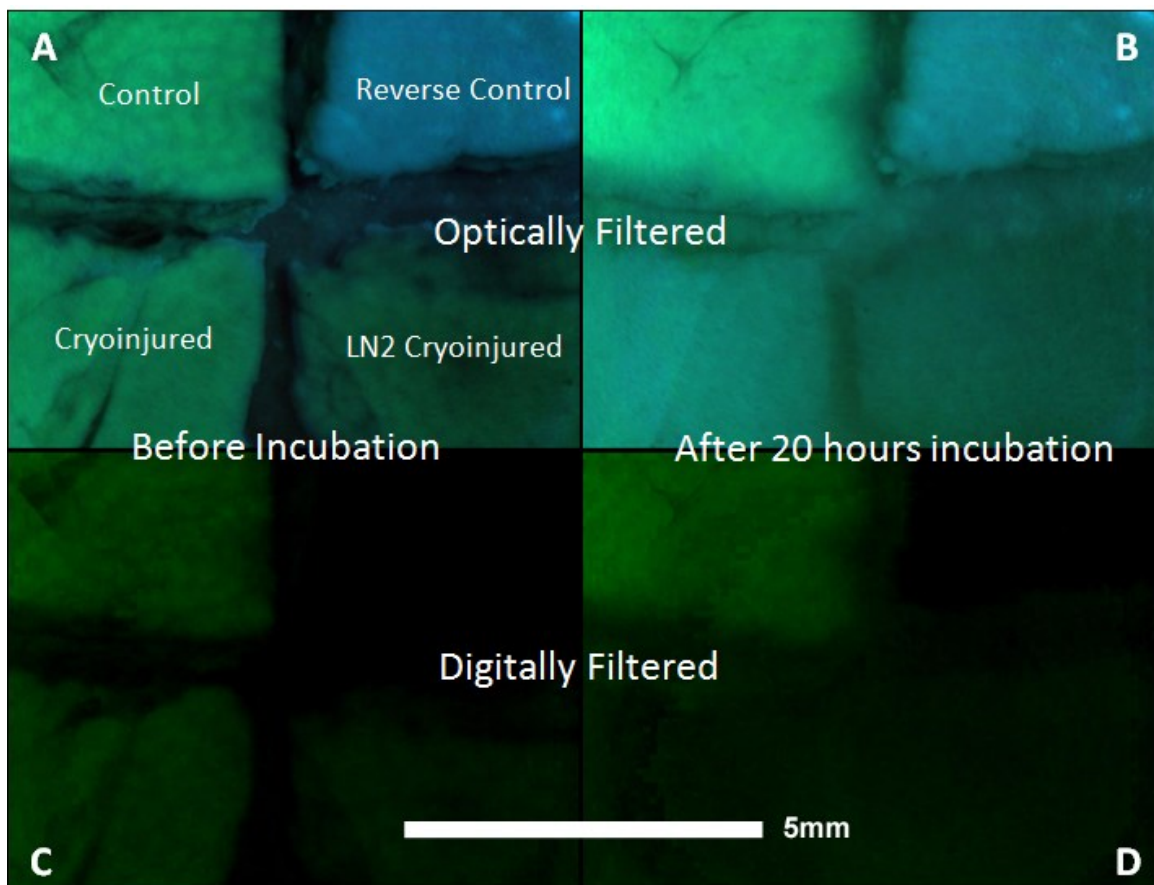


Figure 3.6 - GFP fluorescent intensity for control, reverse control and slow-freeze samples, before and after incubation

Note that the inverse control sample exhibits no green fluorescence, and only reflects back the blue illumination. The other three samples exhibit similar levels of fluorescence. Furthermore, after 20 minutes of incubation, the control sample still exhibited near-full fluorescence, while the two cryoinjured samples exhibited the same level of diminished fluorescence. The denatured sample, as expected, never exhibited any fluorescence throughout the study.

These images shows that all GFP is denatured immediately in the hyperthermal insult case, as previously reported [15], and that no fluorescence is immediately lost following hypothermal insults [14]. They also illustrate that the samples plunged in liquid nitrogen exhibited no measured difference to those frozen using a cryoprobe, indicating that under these conditions both methods completely devitalized the tissue.

3.4.3 Numerical Results

The results of the GFP tissue observation, following cryoinjury, are consistent with what would be expected assuming diffusion of GFP is the mechanism of lost fluorescence. As shown in Figure 3.7, the control sample stays at a relatively constant luminance, while the cryoinjured sample loses approximately 15% of its fluorescence over the 6 hours of the study. Note that the inverse control (denatured sample) is not plotted here, as it exhibited universally zero fluorescence at all times.

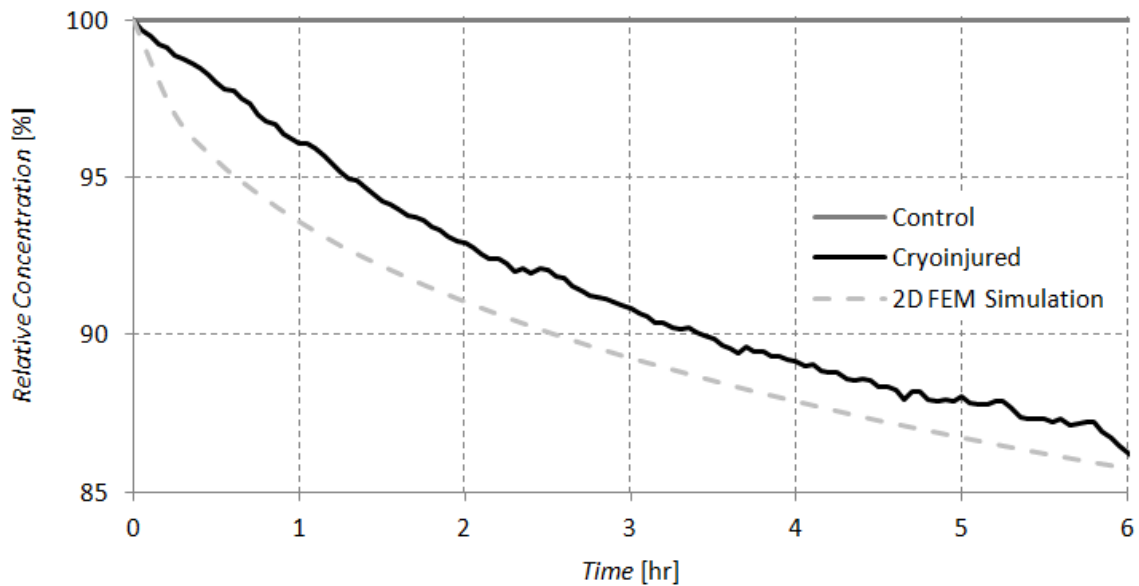


Figure 3.7 - GFP transient fluorescence of a representative sample compared to a 2D COMSOL FEM simulation

The results of the simulation follow the trend of the transient fluorescence of the real tissue. The simulated model does lose fluorescence more rapidly than the tissue, at least, initially.

3.4.4 GFP Conservation

Figure 3.8 shows the fluorescence of the incubation PBS and tissue dissociation with time. Figure 3.8(a) shows that the fluorescence of the incubation PBS for the cryoinjured tissue increases over the first six hours. The increase of GFP in the PBS is due to the loss of GFP from the tissue. It is noted that the control tissue incubated in the PBS also gained some fluorescence over the first 6 hours, although it is a smaller fraction of the fluorescence gained by the PBS containing the cryoinjured tissue. Note that the error bars are large for the PBS samples, as they have relatively very little fluorescence when

compared to the tissue samples. Error bars represent the standard deviation between samples.

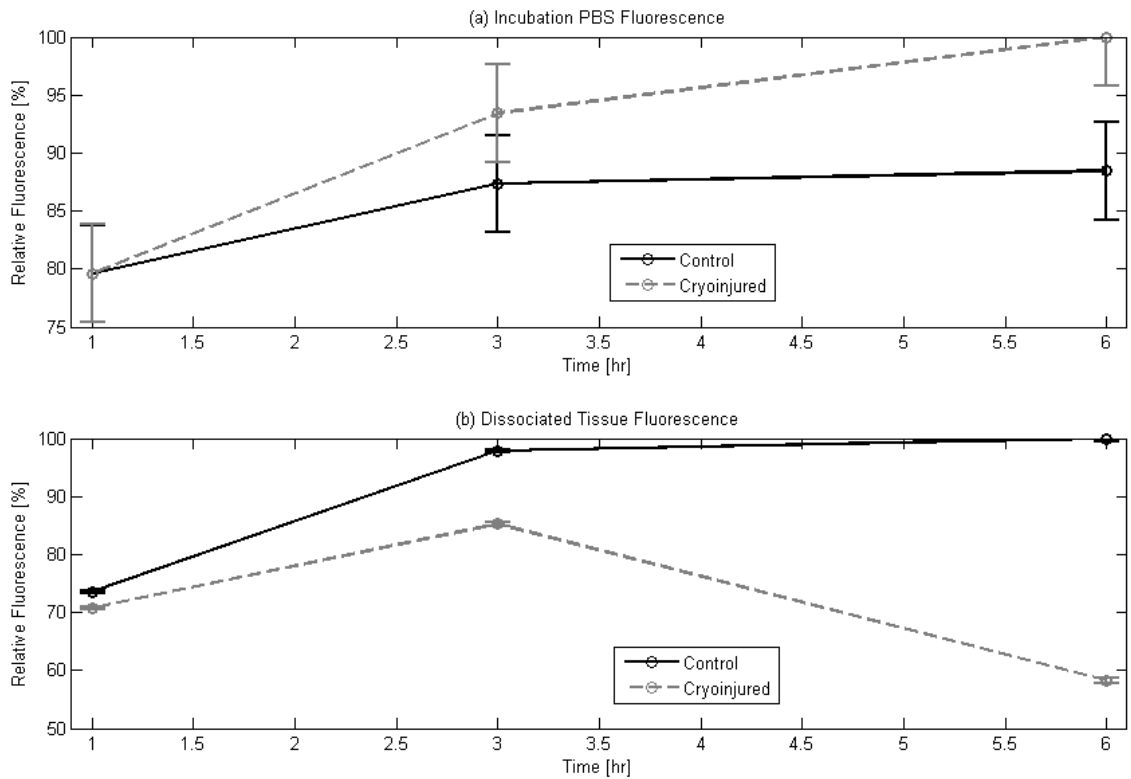


Figure 3.8 – Transient fluorescence during dissociation of incubation PBS (a) and dissociated tissue (b)

The dissociated tissue curves, shown in Figure 3.8(b), have a more interesting behavior. It is expected that the fluorescence of the dissociated control tissue remains constant, while that of the cryoinjured tissue decreases (as the fluorescence of the incubation PBS for the cryoinjured tissue correspondingly increases). While this behavior is observed for times in the experiment beyond the three hour mark, both control tissue and cryoinjured tissue start out gaining fluorescence. It suffices to note that relative to the control tissue, the cryoinjured tissue loses fluorescence at every time step, supporting

the observed increase in fluorescence of the incubation PBS. Error bars again represent the standard deviation between samples.

3.5 Discussion

The results presented in this study are only valid for *ex vivo* cryogenic studies, as it requires both a GFP transfected organism, and relies on long incubation period in an otherwise-static system. It is expected that perfusion in a living system could potentially expedite diffusion results, however this remains untested.

Although the trend of the real tissue follows that of the simulated diffusion model there is some discrepancy between the two. This discrepancy may come from the assumption of zero GFP-concentration at the system's boundaries. Some error may also be due to the magnitude of the GFP diffusion coefficient, which was based on that occurring in a general extracellular matrix and, thus, not necessarily specific to hepatic tissue. These errors are exacerbated by the unknown optical depth of the tissue, hence the results are only valid for observation of a trend, which was done here. Note that the fluorescence of the cryoinjured tissue was only 15% lower than the control tissue after six hours. In reality, this difference will continue to increase given more incubation time, but the difference becomes readily apparent after this period, and further waiting becomes unnecessary.

The motivation of this study was originally to extend the use of GFP as an indicator of cellular viability to viability in whole tissues. In the literature supporting the use of GFP

as a viability assay for cellular suspensions, there is no mention of any time delay between the cellular cryogenic insult, the observed loss of fluorescence, and cellular viability. In contrast, tissue assays exhibit a delayed fluorescent response.

As the driving mechanism of fluorescence loss is diffusion, the difference in single cell and bulk tissue is simply the geometry of the system. A single cell achieves diffusion of GFP very rapidly, while a bulk tissue can require several hours to noticeably exhibit any loss in fluorescent intensity. This difference is illustrated in a comparison of the characteristic time for diffusion between that of single cells (10-50 μm), and that of a bulk (1-100 mm) tissue. A relative comparison between the two length scales can be made through the characteristic time of diffusion equation (Equation 3.3).

Solving for t in the equation, it can be demonstrated that the characteristic time of diffusion over the cellular length scale is on the order of several seconds, while the characteristic time of diffusion over the bulk length scale occurs on the order of several hours. Thus, the loss of GFP fluorescence following cryogenic insult may be fully explained by the onset of diffusion of the GFP molecules from the tissue. This result supports the observation that for a single cell the fluorescence loss following cryoinsult occurs over the course of a few seconds [11], while the fluorescence loss from a network of cells (tissue) occurs over the course of a few hours. Further studies may describe the correlation of tissue size determining the characteristic time of diffusion, and the actual observed changes in fluorescence.

Since all factors typically affecting fluorescence yield, such as exposure duration, excitation light intensity, temperature, pH, were kept constant in this study, the observed fluorescence drop can only be attributed to either one of two factors, or both: 1) GFP diffusion from the affected cells into the surrounding medium and/or 2) intracellular effects leading to cell apoptosis and/or necrosis that ultimately yield GFP diminished fluorescence. As the observed drop in fluorescence corresponds with increased fluorescence in the incubation medium, the second condition alone cannot account for the drop in fluorescence, therefore GFP diffusion appears to be if not the only one, at least the major driving force behind transient fluorescence. Furthermore, the trends of the effective diminished fluorescence of the tissue seem to be well represented by Fick's 2nd law (Figure 3.6), suggesting again that GFP diffusion is, if not the only mechanism responsible for GFP loss, at least the dominant phenomenon. As such, factors which affect the speed of diffusion (geometry, temperature, surrounding fluid, diffusion coefficient, etc.) will greatly affect the required duration of incubation. For example, for the hepatic tissue used in this study, a rectangular parallelepiped with dimensions 6x6x4.4 mm with a diffusion rate of 5.6E-11 m²/s led to an incubation time of approximately 3.5 hours before significant changes in fluorescence could be observed.

3.6 Conclusion

The loss of fluorescence in cryogenically-treated cells and tissues is due to the diffusion of GFP from the cell/tissue onto the surrounding media (extracellular space/medium), onset by the cryogenic insult.

The loss of GFP in cryoinjured tissues will not, however, be immediately apparent, as the diffusion required to show regions of damaged tissue may take hours. The required incubation period for cryoinjured GFP tissues before checking viability will depend on all environmental factors which govern diffusion. Future studies may be dedicated to determining the incubation period required given a variety of research conditions in a variety of tissues. For the samples used in this study, an incubation period of approximately 3.5 hours is sufficient to observe a significant drop in fluorescence (>10%).

Provided the aforementioned precautions and allowances are made, GFP may be successfully used as an indicator of viability in *ex vivo* GFP-transfected cryoinjured tissues. It shares all the same benefits of using GFP as a viability assay in single cells, while only requiring more time to exhibit and obtain the results. As fluorescence can be ascertained *in situ*, GFP as an indicator of viability in cryoinjured tissues can potentially be a valuable technique where more traditional assays may be inappropriate in preclinical trials.

CHAPTER 4 MONTE CARLO METHOD FOR PHOTON HEATING USING TEMPERATURE-DEPENDENT OPTICAL PROPERTIES

Chapter 4 in its entirety, excepting section 4.5, has been submitted for publication in *Computer Methods and Programs in Biomedicine* and is currently under review.

4.1 Abstract

The Monte Carlo method for photon transport is often used to predict the volumetric heating that an optical source will induce inside a tissue or material. This method relies on constant (with respect to temperature) optical properties, specifically the coefficients of scattering and absorption. In reality, optical coefficients are typically temperature-dependent, leading to error in simulation results. The purpose of this study is to develop a method that can incorporate variable properties and accurately simulate systems where the temperature will greatly vary, such as in the case of laser-heating of frozen tissues.

A numerical simulation was developed that utilizes the Monte Carlo method for photon transport to simulate the thermal response of a system that allows temperature-dependent optical and thermal properties. This was done by combining traditional Monte Carlo photon transport with a heat transfer simulation to provide a feedback loop that selects local properties based on current temperatures, for each moment in time. Additionally, photon steps are segmented to accurately obtain path lengths within a homogenous (but not isothermal) material. Validation of the simulation was done using

comparisons to established Monte Carlo simulations using constant properties, and a comparison to the Beer-Lambert law for temperature-variable properties.

The simulation is able to accurately predict the thermal response of a system whose properties can vary with temperature. The difference in results between variable-property and constant property methods for the representative system of laser-heated silicon can become larger than 100 Kelvin. This simulation will return more accurate results of optical irradiation absorption in a material which undergoes a large change in temperature. This increased accuracy in simulated results leads to better thermal predictions in living tissues and can provide enhanced planning and improved experimental and procedural outcomes.

4.2 Introduction

Heating a medium using electromagnetic irradiation is a common technique in a variety of disciplines, ranging from electronics to medicine to welding. There exist numerous applications where electromagnetic heating is intended to induce some thermal damage or structural change in a medium. For example, in medicine, lasers are often used in ablative techniques, where the temperature of the surrounding tissue needs to stay within a certain threshold [25]. Other techniques use laser heating to prevent thermal damage inherent in cryosurgery [2]. While lasers are often used in medicine due to their precision, other irradiative techniques are gaining prominence, such as microwave irradiation [26].

Myriad tools currently exist to simulate the optical distribution within a material, principally using the Beer-Lambert equation to directly determine optical distribution, or Monte-Carlo simulations to determine photon scattering and distribution [27, 28]. No matter the method used, the optical distribution is then used to determine the thermal response of the material to the optical irradiation. These approaches to simulating the optical distribution critically neglect the temperature dependent nature of a material's optical properties.

Current simulation techniques use constant optical properties, often at room temperature, to determine the optical distribution within the material. While this may in practice be a reasonable approximation for materials that do not experience a large change in temperature, this limitation becomes important as thermal gradients become large. This is especially true in the case of a material which undergoes phase change.

Variable Optical Irradiation Distribution Simulation software (VOIDSim) was developed to simulate irradiative heating while using temperature-dependent optical and thermal properties. The software not only will determine the optical distribution within the material, but also will simulate the thermal response of the material to the irradiation. Furthermore, the software is robust enough to allow a variety of irradiative source geometries, temporal irradiative profiles, and an arbitrary system geometry.

4.3 Description of Method

4.3.1 Terminology

The program is called Variable Optical Irradiation Distribution Simulation (VOIDSim). VOIDSim requires the user to define a simulation geometry using a series of CAD files (STL file format), with a single file corresponding to a single material in the simulation. The terminology represented in Figure 4.1 will be referenced in this paper.

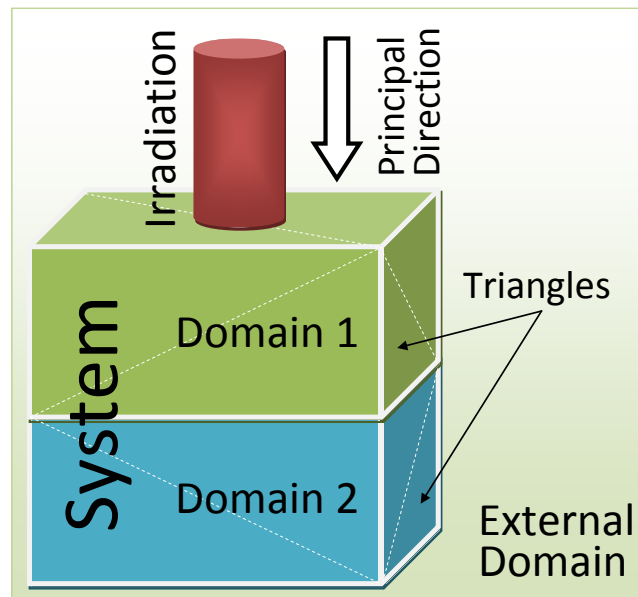


Figure 4.1 - Simulation Terminology

The “system” refers to all modeled solid bodies in the simulation, or rather, all physical domains wherein energy propagation is considered. The system is divided into domains, which share all properties (constant or variable), and at the outset are homogeneous. Each domain is geometrically defined as a collection of outward-pointing triangles which form its surface. Each domain is divided into a regular grid of cells (not

shown in Figure 4.1), with nodes at the center of each cell. Each cell has uniform homogeneous properties at each moment in time.

4.3.2 Program Overview

The program includes Monte Carlo photon tracing algorithms first developed by Prahl *et al.* [27] and expanded upon by Wang *et al.* [28]. As VOIDSim allows for arbitrary geometries (not restricted to a single domain, or horizontal layers) it utilizes ray-tracing techniques, specifically using the ray-triangle intersection algorithm developed by Moller *et al.* [29], to determine angles of incidence with boundaries. The flow diagram for VOIDSim is shown below, in Figure 4.2.

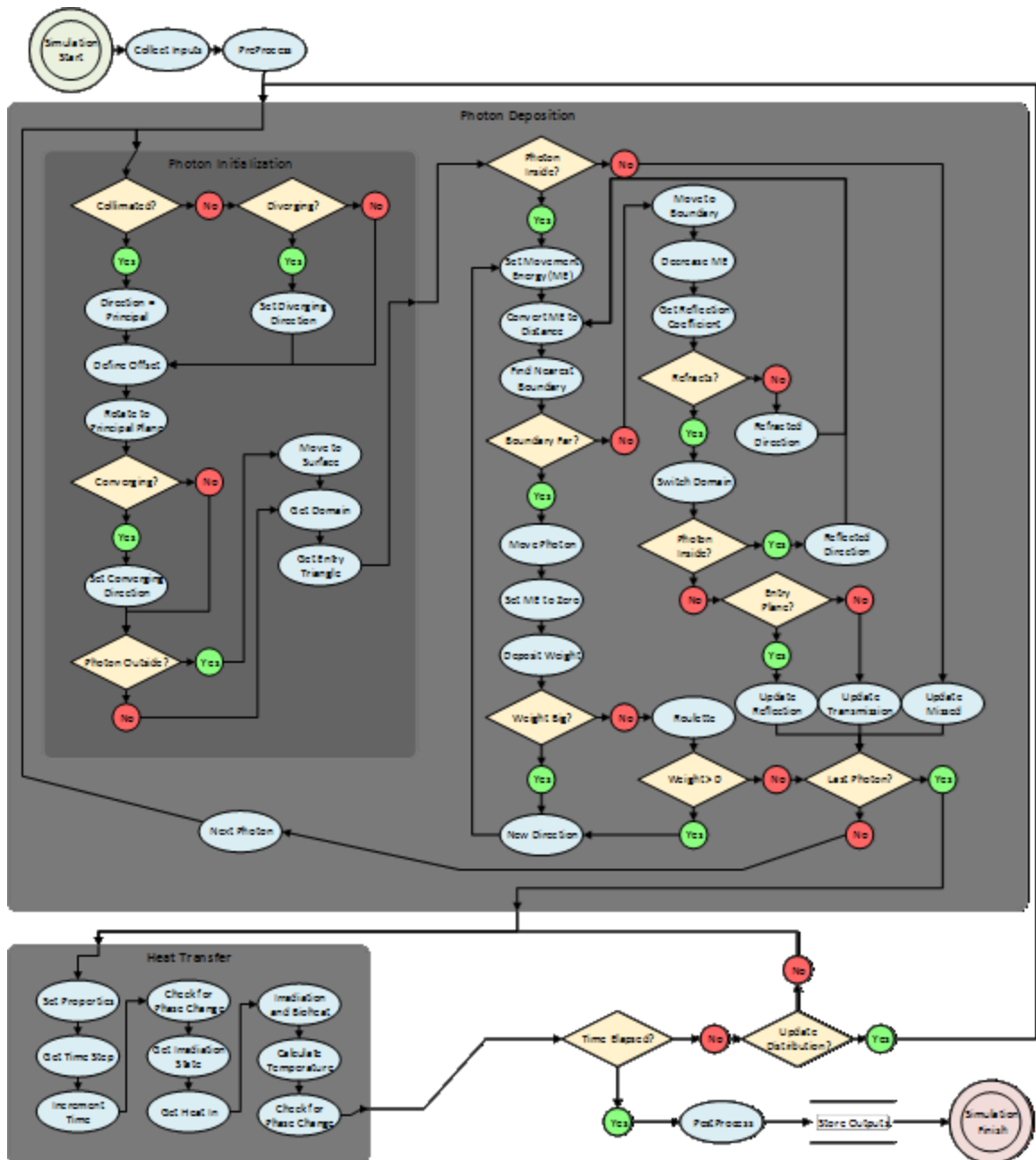


Figure 4.2 - VOIDSim flowchart

Before the program can start, the user must provide the appropriate inputs into the program. VOIDSim provides a form-based user interface based on .NET Winforms. The user specifies all pertinent thermal and optical properties for each domain in the GUI. Variable properties are defined as look-up tables, with each data point requiring the

temperature and property value. VOIDSim utilizes linear interpolation/extrapolation to retrieve properties based on current system temperatures. In the case of extrapolation, if a physically impossible property is derived (e.g. negative thermal conductivity) that property is set to its logical boundary (e.g. thermal conductivity equals zero). Once all required inputs are satisfied, the user may start the simulation.

In preprocessing, the program converts all user inputs to SI units (kilograms, meters, seconds, and Kelvin) to avoid any conversion errors. Memory is allocated for each node in the system, all constants are computed, and the initial system condition is recorded. For n photons “Photon Deposition” occurs, which determines the spatial distribution of a photon packet. Before the distribution can be calculated, the photons must be initialized in their starting locations (“Photon Initialization”). Once Photon Deposition has concluded for n photons, “Heat Transfer” in the system is calculated for an incremented moment in time. The simulation time is updated, and the program returns to Photon Deposition if the update condition requires it, otherwise it proceeds with the next time step of Heat Transfer. Once the user-defined simulation time elapses, the simulation is complete.

The majority of the subroutines in Photon Deposition are similar to those found in MCML [28], for example. Where Photon Deposition majorly differs is its treatment of geometries (to allow for arbitrarily-shaped geometries) and how it incorporates variable optical properties.

4.3.3 *Movement Energies*

Rather than immediately determining the distance a photon will move in a medium, based on the medium's total optical attenuation coefficient, a photon is first given Movement Energy, which is defined as the negative natural log of a random number, between zero and one. This is done to reduce calculations as well as to provide a way for a photon to move in a domain with non-constant optical coefficients.

4.3.4 *Finding the Nearest Boundary*

VOIDSim allows arbitrary geometries, and does not rely on domain boundaries in any particular plane. To achieve this, the photon is assigned to a particular domain, based on its location. Each domain has a set of triangles which define its surface. To determine where the nearest boundary of collision is, a ray-triangle intersection algorithm [29] is used for each of the triangles that belong to the photon's current domain. Exactly one triangle will be intersected by the ray defined by the photon's current location and direction. The distance to this triangle is calculated and used as the distance to the nearest boundary.

4.3.5 *Moving a Photon with Variable Optical Properties*

Determining the distance that a photon will move with a given movement energy must be done on a cell-to-cell basis when optical properties are permitted to vary. First the distance between a photon and its nearest boundary in its current direction is calculated. Then the index of the cell in which the photon is located is determined. The

distance from the photon to the wall of the current cell is also calculated. Finally the total attenuation coefficient for the current cell is interpolated/extrapolated and the distance the photon can move with its current movement energy within the current cell is determined. The photon then moves the least of these three distances, leaving it located in the middle of the cell, on the cell wall, or on the boundary wall. Its movement energy is appropriately discounted, and if any movement energy remains, the process is repeated until either no movement energy remains, or until the photon collides with the domain boundary.

4.3.6 Depositing Weight and Scatter Angles with Variable Optical Properties

To determine the amount of weight deposited, or the appropriate scatter angle, when variable optical properties are used, the local optical property must be determined. First, the photon location is translated into the index of the cell in which it currently resides. The temperature of this cell is then used to determine the absorption and scattering coefficients in the case of weight deposit, or the anisotropy of scattering in the case of getting the scatter angle.

4.3.7 Heat Transfer

Heat transfer is done by dividing the system into individual cells. At each node (the center of each cell), an energy balance based on the non-steady conservation of energy is used. Heat into each node is a summation of conductive heat energy (from surrounding cells), irradiation energy (from photon deposition), volumetric heating and perfusion

(bioheat). Explicit finite difference heat transfer is then used to calculate the subsequent temperatures at each node.

Additionally each cell carries a fusion energy, related to its current physical state (frozen or thawed). In order for a cell to change temperature from a frozen to thawed state (or vice versa), the heat into each node is first used to provide/take the required fusion energy for the change in physical state. Any leftover heat after fusion energy saturates (or depletes) is used to change the cell's temperature.

4.4 Validation

4.4.1 Photon Deposition with Constant Optical Properties

The algorithms in VOIDSim utilize the same underlying mathematical approximations to physical phenomena that several other existing Monte-Carlo based simulations use. As such, results from VOIDSim should be identical (within a statistical distribution) when identical properties and geometry are used with each simulation. The three test cases that Wang *et al.* [28] used for validation were also used to validate VOIDSim results. The first is a semi-infinite slab of material, with irradiation incident normal to its surface. The results are compared to various classic simulations in Table 4.1.

Semi-infinite slab, Conditions			
Index of Refraction	Absorption Coefficient [cm^{-1}]	Scattering Coefficient [cm^{-1}]	Anisotropy of Scattering
1.5	10	90	0 (isotropic)

Semi-infinite slab, Results		
Source	Reflectance	Photons
Giovanelli [30]	0.2600	N/A
Wang et al. [28]	0.25907	50,000
Prahl et al., 1989 [27]	0.26079	50,000
VOIDSim	0.25891	500,000

Table 4.1 – Semi-infinite slab reflectance

As shown in Table 4.1, there is close agreement of the steady state reflectance for each of the studies shown. The largest relative difference between VOIDSim results and any other study is 0.72%.

Slab, Conditions				
Index of Refraction	Absorption Coefficient [cm⁻¹]	Scattering Coefficient [cm⁻¹]	Anisotropy of Scattering	Thickness [mm]
1	10	90	0.75	0.2

Slab, Results			
Source	Diffuse Reflectance	Transmittance	Number of Photons
van de Hulst [31]	0.09739	0.66096	N/A
Wang <i>et al.</i> [28]	0.09734	0.66096	500,000
Prahl <i>et al.</i> [27]	0.09711	0.66159	500,000
VOIDSim	0.09753	0.66111	5,000,000

Table 4.2 - Thin-slab reflectance and transmittance

Table 4.2 represents a simulation where the boundary condition (refractive index) is now matched with the external refractive index, and the slab is now thin enough (two optical depths thick) for irradiation to partially pass through. The irradiation is again normally-incident upon the surface of the slab. There is an even closer alignment of the results from VOIDSim and those of the other simulations. The largest relative difference for reflection and transmission are 0.43% and 0.07%, respectively.

Multi-layer, Conditions					
Layer ID	Index of Refraction	Absorption Coefficient [cm ⁻¹]	Scattering Coefficient [cm ⁻¹]	Anisotropy of Scattering	Layer Thickness [mm]
1	1.37	1	100	0.9	1
2	1.37	1	10	0 (isotropic)	1
3	1.37	2	10	0.7	2

Multi-layer, Results			
Source	Diffuse Reflectance	Transmittance	Number of Photons
Gardner <i>et al.</i> [32]	0.2381	0.0974	100,000
Wang <i>et al.</i> [28]	0.2375	0.0965	1,000,000
VOIDSim	0.2382	0.0951	10,000,000

Table 4.3 - Multiple layers reflection and transmission

Finally, there is the comparison to multiple stacked layers (Table 4.3), with irradiation normally-incident upon the outside surface of the first layer. The largest relative errors for reflection and transmission are 0.29% and 2.36%, respectively.

4.4.2 Photon Deposition with Variable Optical Properties

For this validation, a system consisting of a single domain in the shape of a cube with sides of 1 cm will be used. The simulated material is silicon, with variable optical properties as shown in Table 4.4 (from [33]) and constant properties as shown in Table 4.5.

Temperature [K]	Absorption Coefficient [cm ⁻¹]
298	0.15
363	0.40
415	1.8
473	5.7

Table 4.4 - Optical absorption coefficient of silicon at 1180 nm

Thermal Conductivity [W/m·K]	149
Specific Heat [J/kg·K]	700
Density [kg/m ³]	2329
Scattering Coefficient [cm ⁻¹]	0.001
Anisotropy of Scattering	0.9
Refractive Index	1

Table 4.5 - Constant properties of silicon

For this simulation a collimated circular-profile laser with 0.5 cm diameter and power of 70 watts will be directed towards the $z = 0$ surface of the cube. The cube will be irradiated continuously for 10 seconds. Due to the high thermal diffusivity of silicon ($91 \text{ mm}^2 \cdot \text{s}^{-1}$) and small size of the system, the temperature of the system will be treated as homogenous, and a lumped-capacitance heating model may be used.

The simulation evaluated using VOIDSim is compared to the Beer-Lambert law of absorption, shown in Equation 4.1, where A is the absorption, $\mu_a(T)$ and μ_s are the absorption and scattering coefficients (μ_a being a function of temperature), respectively, and ℓ is the thickness of the material. R_{sp} is the specular reflection, and as this simulation uses matched boundary conditions (refractive index of system and external domain both equal one) it is equal to zero.

$$A(T) = (1 - R_{sp})(1 - e^{-(\mu_a(T) + \mu_s)\ell})$$

Equation 4.1 - Beer-Lambert law for absorption

Once the absorption is known, then it can be multiplied by the energy into the system to determine the proceeding temperature. Equation 4.2 represents the algorithm for determining the subsequent temperature of the system, where dT is the differential

temperature, dt is the differential time, P is the laser power, ρ is the density of the material, V is the volume of the material, and c is the specific heat of the material.

$$\frac{dT}{dt} = \frac{A(T)P}{\rho V c}$$

Equation 4.2 - Lumped-capacitance ODE

The Euler method, with a step size of 0.1 s, is used to solve the ODE for both a constant absorption coefficient as well as an absorption coefficient that is continuously reevaluated based on the current temperature, utilizing linear interpolation of Table 4.4.

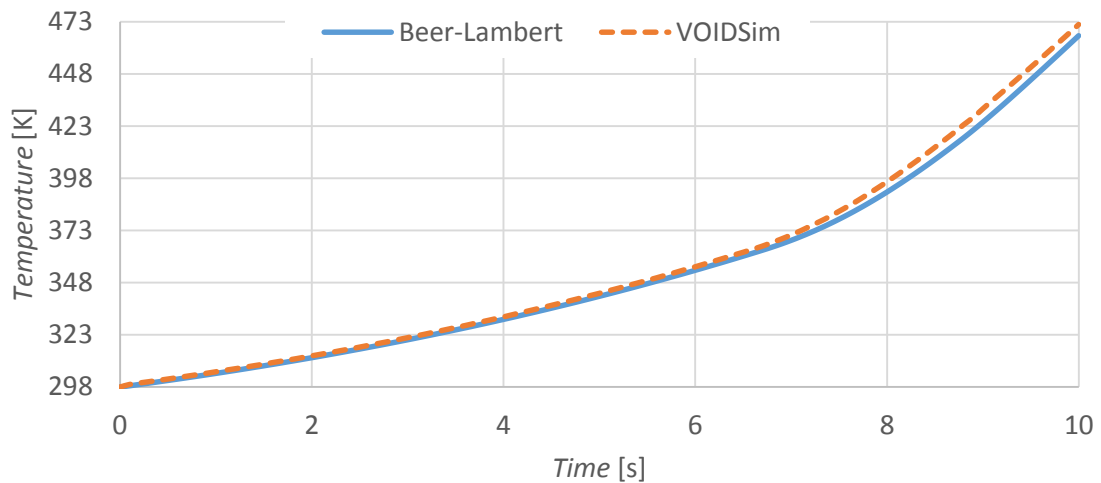


Figure 4.3 – Temperature using variable absorption coefficients

Figure 4.3 shows the temperatures of the silicon cube using both VOIDSim and the Beer-Lambert law. The difference between the methods shows a maximum relative error of 1.52% at any moment in time.

4.5 Heat Transfer

To demonstrate that the simulation accurately portrays heat transfer, several separate simulations were performed, which independently confirm the validity of each

particular phenomenon they represent. Each of these independent confirmations taken as a whole, validate the heat transfer portion of the simulation in its entirety.

4.5.1 Heat Transfer in Three Dimensions

To validate that the algorithms for determining transient heat transfer in three dimensions are accurate, a simulation evaluated using VOIDSim was compared with an identical simulation evaluated using COMSOL Multiphysics software.

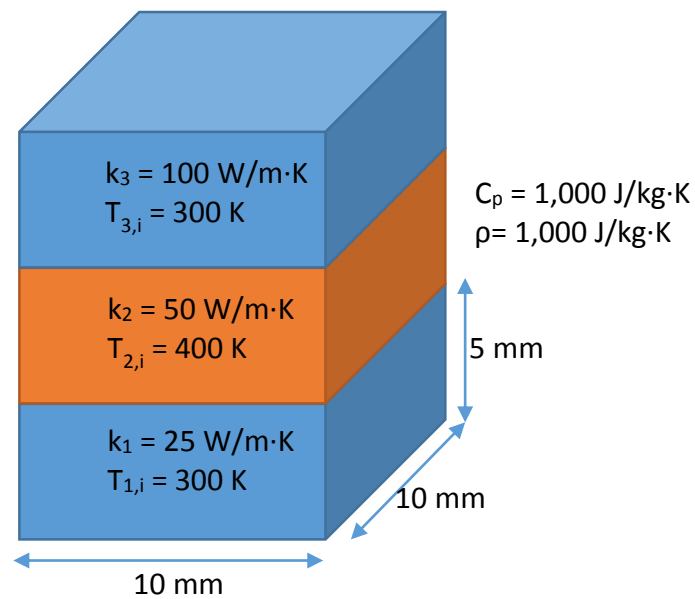


Figure 4.4 - System geometry and properties

The simulation consists of the system shown in Figure 4.4. Each domain has identical specific heats, densities, and dimensions. From bottom to top the domains will be referred to as z1, z2, and z3. The initial temperature and thermal conductivity for each domain are as shown.

The simulation was performed over 0.2 seconds, with resolution of 0.005 seconds between solution times for VOIDSim. The temperatures at the midpoints of each solid are plotted for each solution time in Figure 4.5.

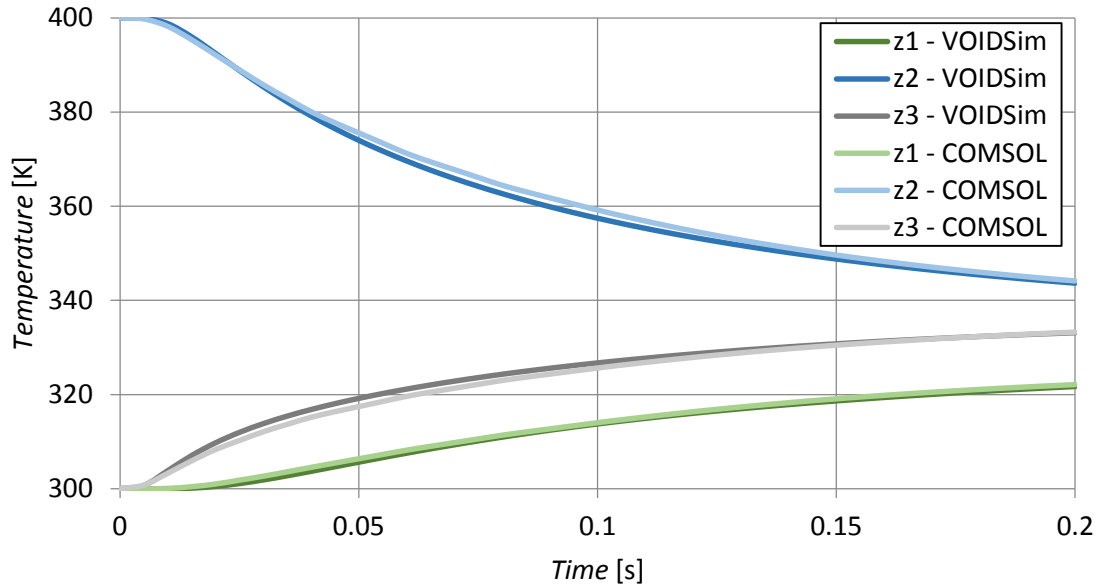


Figure 4.5 - 3D heat transfer comparison

As shown, there is close agreement between the VOIDSim solution and the COMSOL solution. At each point in time, the maximum disagreement between any of the temperatures is 1.90 K, with the average difference being 0.78 K, with an average standard deviation of 0.55 K. This is taken as evidence that heat transfer in three dimensions provides correct results within a reasonable tolerance.

4.5.2 Heat Transfer with Volumetric Heat Generation

To demonstrate that VOIDSim properly handles volumetric heat generation (e.g. metabolism) and volumetric heat distribution from laser heating, the COMSOL model was

slightly modified, so that z1 now included volumetric heat generation, with a value of $1.0E8 \text{ W/m}^3$. The large value was chosen due to the short simulation duration (0.2 seconds). All other properties remain the same as before (see Figure 4.4). Again the domain midpoint temperatures were plotted, and those results are shown in Figure 4.6.

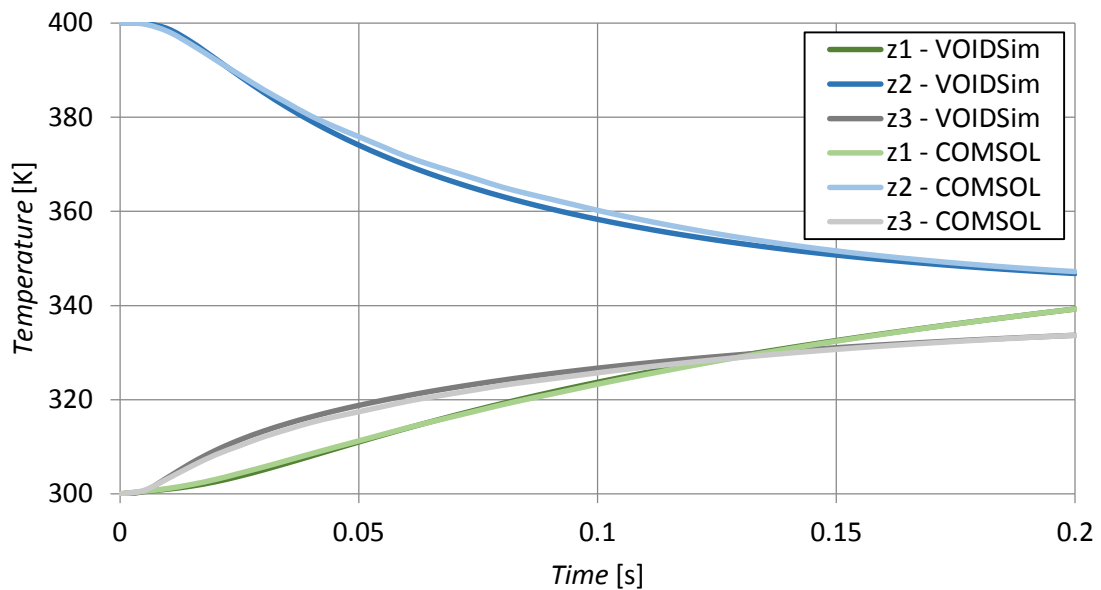


Figure 4.6 - Volumetric Heat Generation Midpoint Temperatures

As seen, the heat generation term affected z2 and z3 very little (no volumetric generation), but served to significantly heat z1. The maximum difference between the COMSOL and VOIDSim models for z1 at any time step was 0.55 K, with the average difference being 0.25 K and the average standard deviation being 0.18 K.

4.5.3 Heat Transfer with Phase Change

COMSOL was also utilized to compare VOIDSim heat transfer results where a phase change takes place. Although COMSOL approximates the changes in properties and

latent heat of fusion with step and Dirac delta functions, it is still a useful, if inaccurate, approximation. The COMSOL simulation is borrowed from the COMSOL Model Gallery (model 474) [34]. The properties of the COMSOL simulation vary with temperature, whereas the properties in VOIDSim are held constant for each phase, with an abrupt change at the transition temperature.

The simulation geometry is a square rod of ice, 0.01 m in length, and initially at 253 K. The diameter of the rod is large enough to make the problem one-dimensional. The far end of the rod ($x = 0.01$ m) is held at a constant 353 K, and all other surfaces are thermally insulated. The properties use for the ice/water are listed in Table 4.6.

Phase	Specific Heat [J/kg·K]	Density [kg/m³]	Conductivity [W/m·K]
Ice	2,052	918	2.31
Water	4,179	997	0.613

Table 4.6 - Thermal properties of water in two phases

The enthalpy of fusion used is 333,500 J/kg. The same model was solved using both VOIDSim and COMSOL, first considering phase change physics, and again omitting the latent heat of fusion. The results of the simulations are shown in Figure 4.7.

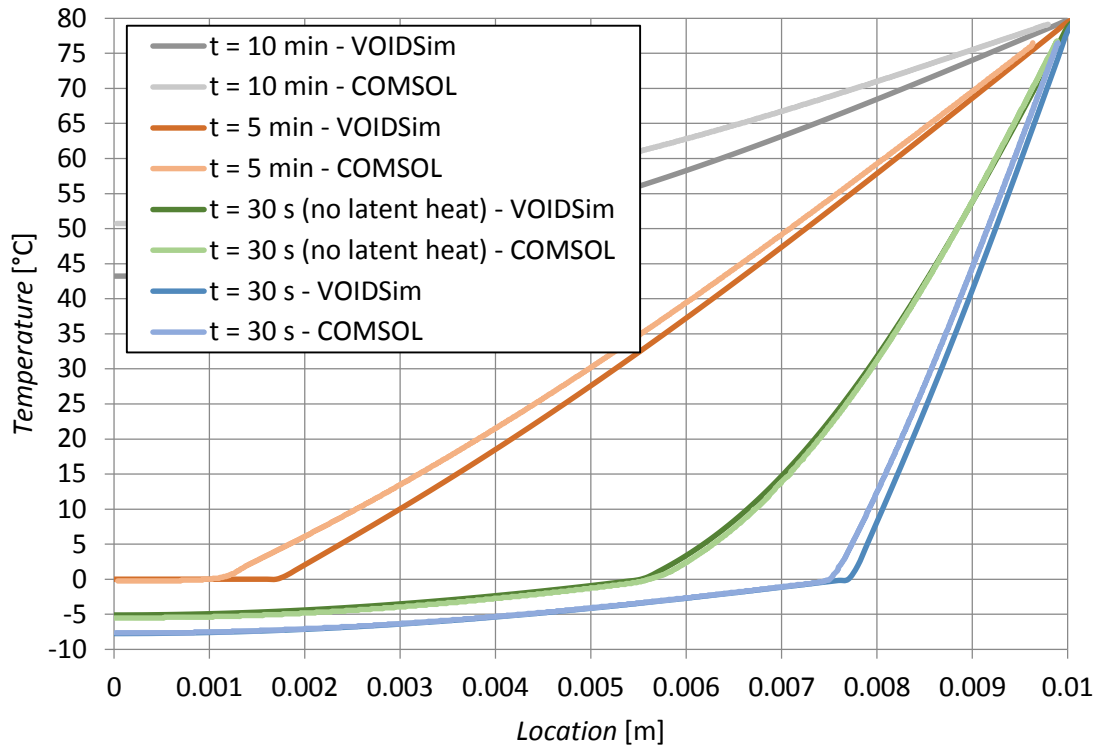


Figure 4.7 - Phase change heat transfer comparison

Figure 4.7 shows very close agreement between models that do not include latent heat of fusion. The introduction of latent heat slows the temperature change of the ice rod as expected, although there is slight disagreement between VOIDSim and COMSOL results. The discrepancy is likely due to the properties of the COMSOL model varying with temperature. Overall there is sufficient evidence that VOIDSim does implement phase change simulation correctly and with reasonable accuracy.

4.6 Representative Simulation

To demonstrate the benefit of using VOIDSim over current Monte Carlo photon propagation simulations, a simple representative simulation was done. For this simulation an identical silicon cube is used, with identical properties and parameters as previously

described (4.4.2). The refractive index of the silicon is changed from 1 to 3.5, and the laser power is changed to 80 watts. These parameters are similar to what might be seen in a real-life silicon machining process. Again the temperature of the cube is assumed to be isothermal. The simulation will be done for two cases. The first will represent a traditional analysis, assuming a constant absorption coefficient, using the value at room temperature. The second will utilize variable absorption coefficients. The center temperature of each simulation is plotted with respect to time, below in Figure 4.8.

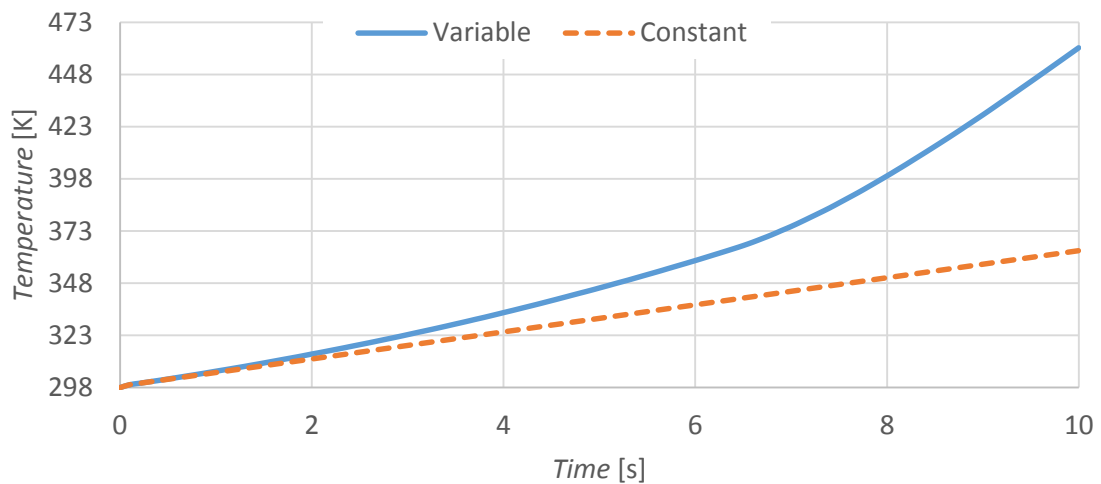


Figure 4.8 - Temperature using variable and constant absorption coefficients

4.7 Discussion and Conclusion

As exhibited by the small differences between results of VOIDSim and various established methods, VOIDSim can accurately simulate photon propagation. Also it has been demonstrated that the difference between VOIDSim results for heat transfer, and the results of established multiphysics simulations, is negligible. Furthermore, it has been

demonstrated that VOIDSim has the ability to correct significant error that exists in a simulation where constant optical properties are assumed.

For the representative simulation shown in Figure 4.8, both the VOIDSim and the Beer-Lambert law curves start heating at the same rate, as both initially absorb the same amount of incident irradiation. As the variable-property simulation (VOIDSim) heats up, however, the absorption coefficient also increases, leading to greater absorption and faster heating. The two curves diverge, as the constant-property simulation (Beer-Lambert) will always absorb the same percentage of incoming irradiation, while the variable-property simulation absorbs nearly all available irradiation as it warms up.

There is a difference of over 100 K between the two curves after 10 seconds, and this difference will become larger as time goes on. While this temperature difference in a manufacturing process may be unimportant, small changes in temperature can be critical in the heating of biological materials. As a simulation does not currently exist that allows accurate prediction of system temperature where variable properties are used, the capabilities of VOIDSim become paramount in applications where optical properties vary with temperature.

VOIDSim was initially developed to simulate the thermal response of frozen tissue to laser heating. VOIDSim allows for the accurate depiction of photon transport in systems that undergo large changes in temperature, and hence, large changes in optical properties. Especially when considering living biological tissues, even small discrepancies

in simulated temperatures can literally mean life and death. VOIDSim alleviates the discrepancies introduced by the assumption of constant optical properties, potentially leading to better experimental and clinical planning, and more favorable outcomes.

The VOIDSim software is available upon request, and the user's manual for the software comprises the entirety of Appendix A.

CHAPTER 5 DISCUSSION AND CONCLUSION

5.1 Discussion

5.1.1 Thermally Induced Fracture of Tissue

The underlying motive of developing VOIDSim software was that there existed no way to accurately predict the thermal profile of a tissue during rapid heating during phase change. The desire to characterize this rapid heating stemmed from a research proposal to develop what is called Thermally Induced Fracture of Tissue (TIFT). This proposal, presented in ASLMS 2012, is a technique to inhibit heat transfer across a tumor's boundary during cryosurgery. If a thermal boundary can be introduced on the surface of a tumor, for example, then the tumor can be cooled to a very low temperature without affecting/freezing the tissue on the other side of the thermal boundary. This ensures complete tumor destruction while maintaining viability of surrounding tissues, reducing or eliminating collateral damage (Figure 5.1).

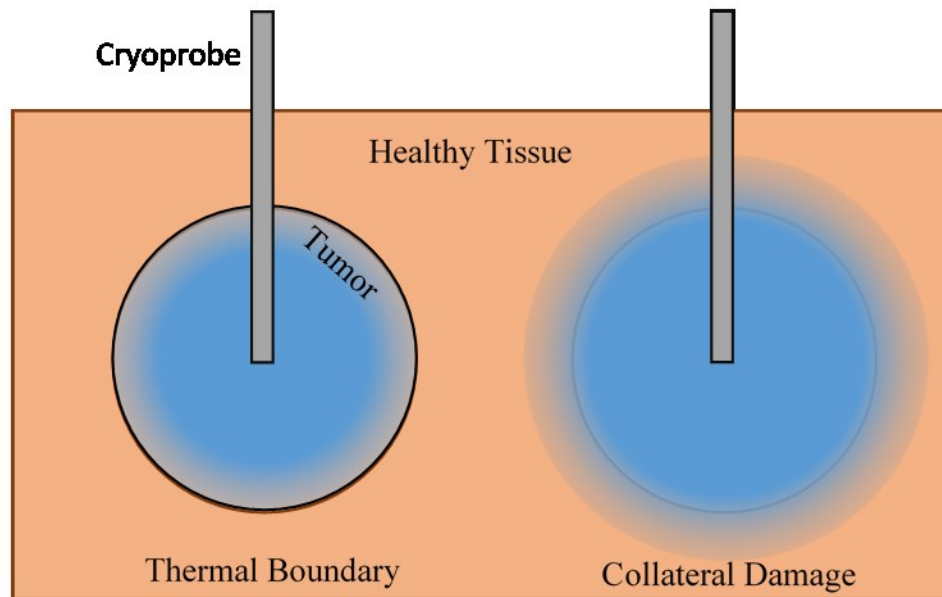


Figure 5.1 – Cryosurgery with thermal boundary (black) from TIFT

To achieve the creation of this thermal boundary a physical discontinuity (fracture) is introduced on the surface of a growing ice-ball, just as it extends past the surface of a tumor. The fracture is introduced from rapid thermal expansion, which induces stresses, and ultimately, fracture. The rapid thermal expansion is achieved through rapid heating via optical irradiation (i.e. laser-heating). The fracture then acts as a thermal discontinuity, and becomes an impediment to the transfer of heat (Figure 5.2).

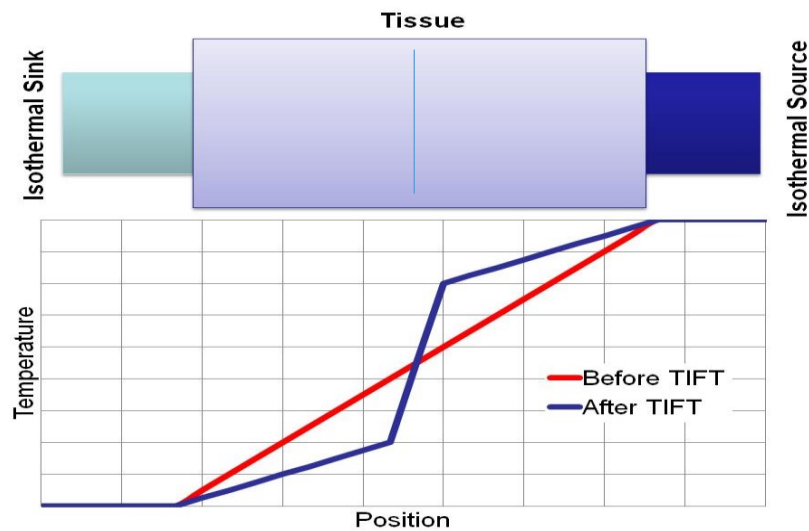


Figure 5.2 - Thermal profile before and after thermal fracture. Thermal boundary from the fracture creates a higher thermal gradient at the location of fracture, allowing better thermal isolation of one side from the other.

It was observed that thermally-induced fractures could be created by plunge cooling or plunge heating small tissue samples. As a first step in this research, it was desired to determine the required heat flux within a target tissue. The required heat flux was measured through convective heating methods (plunge-cooling warm agarose gelatins and plunge-heating cold gelatins). Thermocouples were spaced regularly along a central axis of the sample, and the temperature history was recorded as the sample was immersed in the heating/cooling liquid. A representative sample of the heat flux data is seen in Figure 5.3.

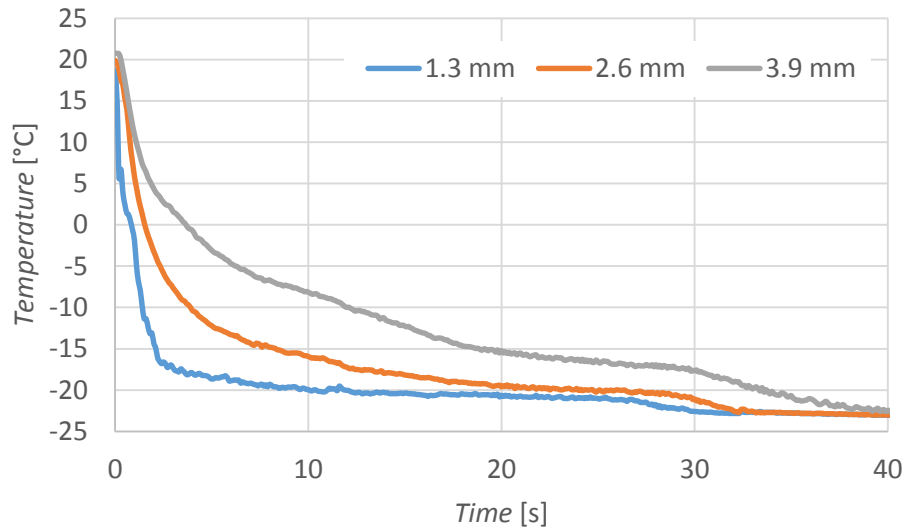


Figure 5.3 - Temperature profile of 8 mm agarose gelatin cube plunge-cooled in tetrafluoroethane. Fracture occurs at approximately 27 seconds. Each thermocouple is placed along the central axis, and distances are from the surface of the cube.

The task then becomes matching the thermal fluxes experienced in fracturing gelatins, this time using laser heating. Applying optical irradiation to induce the same thermal fluxes proved to be impractical through blind experimentation, as the list of variables associated with optical irradiation are numerous. These variables include the laser wavelength, power, pulse width, pulse duration, geometry, etc. To determine the necessary application of optical irradiation to duplicate the thermal profiles seen in convective heating, VOIDSim was developed to enable a researcher to quickly change parameters.

While the proposed study remains feasible, ultimately, constraints on resources (principally time) temporarily sidelined the project. It still remains to duplicate the

thermally-induced fracture with laser heating, and to characterize the effect on heat transfer of the resulting fracture.

5.1.2 *Future Directions*

GFP transfected tissue has been shown to accurately indicate the regions of cryoinjury within *ex vivo* mouse hepatic tissue. Naturally there remains to check that this correlation exists within other varieties (non-hepatic) of tissue, and in particular, for *in vivo* tissues. It is expected that GFP transfected tissues would be even more beneficial in an *in vivo* environment, as the circulatory system of the organism will aid with the diffusion of GFP out of a thermally compromised area. Although utility of this method is limited to GFP-transfected organisms, it can be used to expedite cryoinjury results in a laboratory setting.

VOIDSim software may be used as a tool in myriad applications of laser-tissue interactions over a wide range of temperatures. To facilitate the use of VOIDSim, it is paramount that accurate tissue properties are provided to the software. While the optical properties of tissues are widely reported in the literature based on wavelength of irradiation, there exists little information (outside of semiconductors and water) on the dependency that optical properties have on temperature. Especially in the case of cryogenic laser-tissue interactions, these material properties must be ascertained before accurate characterization of optical transport within the tissue may occur. Once the optical properties of a tissue are known, with their dependence on both wavelength and

temperature, VOIDSim software can simulate the thermal response to any conceivable situation within normal operating conditions.

VOIDSim software can be easily modified to simulate other desired phenomena that depend on thermal histories, such as tissue viability, or thermally-induced stresses. As the time-temperature profile of the system is known, an Arrhenius equation could be used to model tissue viability, or rather, the rate at which proteins unfold and the tissue becomes non-viable could be predicted. The model would have to be significantly altered to model viability for low-temperature tissue viability, as cellular death is no longer a function of protein destruction, but of intracellular ice formation and dehydration. As it is a numerical simulation, VOIDSim could easily be modified to match empirical data in the frozen regimes, and provide a reasonable estimate of viability in laser-irradiated cryogenic tissues.

5.2 Conclusion

The goal of the work represented by this dissertation was to enhance cryosurgery through visualization of cryoinjury, and through the mitigation of cryosurgery's negative side-effects. Chapter 2 dealt with using laser-heating to counterbalance cryosurgery and protect healthy regions of tissue. Chapter 3 regards using Green Fluorescent Proteins in tissues as a reliable indicator of cryoinjury. Chapter 4 deals with accurately simulating laser-tissue interactions, with a focus on cryosurgery.

5.2.1 *Laser-Assisted Cryosurgery*

To show that laser-heating could be used to counteract the freezing front propagation during cryosurgery, a one-dimensional physical model was used with laser heating on one side, and cryogenic cooling on the other. Following the experiment, viability of the tissue was measured. It was determined that using lasers to counteract cryogenic cooling is a viable method of isolating tissues targeted for destruction from surrounding tissues.

5.2.2 *GFP as an Indicator of Cryoinjury*

GFP-transfected tissues were observed to hold an apparent correlation with viability in tissues. This correlation was previously known for individual cells transfected with GFP, but the mechanism by which fluorescence was lost was unknown, and it remained to establish this correlation in bulk tissues. It was observed that tissues gradually lost fluorescence following a cryoinsult. It was theorized that this loss in fluorescence was due to the diffusion of GFP. GFP-transfected tissues were continuously monitored to determine the transient profile of fluorescence. Other phenomena that affect fluorescence were monitored, and it was determined that they were sufficiently constant as to not account for the observed changes in fluorescence. Furthermore, GFP was traced from its origin within tissues to the surrounding medium, and thus it was shown that cryoinjured tissue does lose GFP to its surroundings, while healthy tissue does not. It was shown that GFP fluorescence is likely lost from a tissue due to diffusion, and

that GFP can be used as an indicator of cryoinjury, as long as conditions are favorable for diffusion.

5.2.3 Monte Carlo Method for Photon Heating using Temperature-Dependent Properties

Previously, no known tools existed that were able to simulate light transport, and the thermal response, in tissues of arbitrary geometry. More importantly, existing simulations assumed optical properties to be constant, thus introducing a large source of error in final predictions. To determine the laser-induced heat transfer in a tissue undergoing large changes in temperature, a custom built software program was developed. This program dynamically couples the light transport and heat transport of a system, so as to utilize temperature dependent optical properties.

The software was validated by comparison to existing numerical methods and through comparison to fundamental laws. The validity of the simulation results is evidenced by its close correlation to these standards. It was shown that this simulation can lead to magnitudes of improvements in simulation accuracy, when accounting for variable optical properties.

5.2.4 Significance

The wider-world significance of the research presented in this dissertation is challenging to characterize. While no research done here represents a single revolutionary leap forward in scientific progress, each project does serve to significantly advance current knowledge. More importantly, this research provides tools for others to

enhance their research within the field of cryosurgery and laser-tissue interactions. Using GFP as an indicator of cryoinjury can tell a researcher in a matter of minutes or hours the regions of cryogenic damage in a tissue. Utilizing VOIDSim software enables a researcher to accurately predict the thermal response of their laser-irradiated system. In the case of TIFT, laser parameters can more quickly be deduced that will induce the desired thermal profiles. None of these tools are specific to a certain set of conditions, and may be easily adapted to suit many varied geometries and situations, with limitless potential.

BIBLIOGRAPHY

1. Slade AB, Martínez-Suástegui L, Vié F, Aguilar G: **Green Fluorescent Protein as an Indicator of Cryoinjury in Tissues.** *Annals of Biomedical Engineering* 2013, **41**(12):2676-2686.
2. Martinez-Suastegui L, Duperray B, Godinez F, Guillen G, Slade A, Aguilar G: **Laser-assisted cryosurgery in ex vivo mice hepatic tissue: viability assays using green fluorescent protein.** *Ann Biomed Eng* 2011, **39**(2):636-648.
3. Mazur P: **The role of intracellular freezing in the death of cells cooled at supraoptimal rates.** *Cryobiology* 1977, **14**(3):251-272.
4. Dawber R, Colver G, Jackson A: *Cutaneous Surgery: Principles and Practice.* London: Martin Dunitz; 1997.
5. Cooper SM, Dawber RPR: **The history of cryosurgery.** *Journal of the Royal Society of Medicine* 2001, **94**(4):196-201.
6. **Cryotherapy for the Treatment of Prostate Cancer**
[<http://www.mcw.edu/urology/UrologyNewsletter/June-2011/Cryotherapy-Treatment-of-Prost.htm>]
7. Muldrew K, Hurtig M, Novak K, Schachar N, McGann LE: **Localization of freezing injury in articular cartilage.** In *Cryobiology. Volume 31.* United States; 1994: 31-38.[vol 1].
8. Yang H, Acker J, Chen A, McGann L: **In situ assessment of cell viability.** In *Cell Transplant. Volume 7.* United States; 1998: 443-451.[vol 5].
9. Schreer A, Tinson C, Sherry JP, Schirmer K: **Application of Alamar blue/5-carboxyfluorescein diacetate acetoxymethyl ester as a noninvasive cell viability assay in primary hepatocytes from rainbow trout.** *Analytical Biochemistry* 2005, **344**(1):76-85.

10. Ericsson M Fau - Hanstorp D, Hanstorp D Fau - Hagberg P, Hagberg P Fau - Enger J, Enger J Fau - Nystrom T, Nystrom T: **Sorting out bacterial viability with optical tweezers.** (0021-9193 (Print)).
11. Elliott G Fau - McGrath J, McGrath J Fau - Crockett-Torabi E, Crockett-Torabi E: **Green fluorescent protein: A novel viability assay for cryobiological applications.** (0011-2240 (Print)).
12. Youvan DC, Michel-Beyerle ME: **Structure and Fluorescence Mechanism of GFP.** *Nature Biotechnology* 1996(14):1219-1220.
13. Alkaabi, Klaithem M, Yafea, Abeer, Salman A, S: *Effect of pH on thermal-and chemical-induced denaturation of GFP.* Heidelberg, ALLEMAGNE: Springer; 2005.
14. Leiderman P, Huppert D, Agmon N: **Transition in the temperature-dependence of GFP fluorescence: from proton wires to proton exit.** In *Biophys J. Volume 90.* United States; 2006: 1009-1018.[vol 3].
15. Nagy A, Málnási-Csizmadia A, Somogyi B, Lo, amp, x030B, rinczy D: **Thermal stability of chemically denatured green fluorescent protein (GFP): A preliminary study.** *Thermochimica Acta* 2004, **410**(1–2):161-163.
16. Campbell TN, Choy FYM: **The Effect of pH on Green Fluorescent Protein: a Brief Review.** *Molecular Biology Today* 2001, **2**(1):1-4.
17. Strebel A, Harr T, Bachmann F, Wernli M, Erb P: **Green fluorescent protein as a novel tool to measure apoptosis and necrosis.** *Cytometry* 2001, **43**(2):126-133.
18. **Spectral** **Profiles**
[\[http://www.microscopyu.com/tutorials/flash/spectralprofiles/index.html\]](http://www.microscopyu.com/tutorials/flash/spectralprofiles/index.html)

19. Schaefer BC, Schaefer ML, Kappler JW, Marrack P, Kedl RM: **Observation of antigen-dependent CD8+ T-cell/ dendritic cell interactions in vivo.** *Cellular Immunology* 2001, **214**(2):110-122.
20. Swaminathan R, Hoang CP, Verkman AS: **Photobleaching recovery and anisotropy decay of green fluorescent protein GFP-S65T in solution and cells: cytoplasmic viscosity probed by green fluorescent protein translational and rotational diffusion.** *Biophys J* 1997, **72**(4):1900-1907.
21. **Mobility of Molecules and Particles within the Cytoplasm of a Living Cell** [[http://www.zeiss.de/C12567BE00472A5C/EmbedTitelIntern/Application_Cellular_Cytoplasm/\\$File/CELLMEASURE2.PDF](http://www.zeiss.de/C12567BE00472A5C/EmbedTitelIntern/Application_Cellular_Cytoplasm/$File/CELLMEASURE2.PDF)]
22. Houtsmuller AB: **Fluorescence recovery after photobleaching: application to nuclear proteins.** *Advances in biochemical engineering/biotechnology* 2005, **95**:177-199.
23. Wachsmuth M, Waldeck W, Langowski J: **Anomalous diffusion of fluorescent probes inside living cell nuclei investigated by spatially-resolved fluorescence correlation spectroscopy.** *Journal of Molecular Biology* 2000, **298**(4):677-689.
24. Saito N, Zhao M, Li L, Baranov E, Yang M, Ohta Y, Katsuoka K, Penman S, Hoffman RM: **High efficiency genetic modification of hair follicles and growing hair shafts.** *Proceedings of the National Academy of Sciences* 2002, **99**(20):13120-13124.
25. Starr PA, Vitek JL, Bakay RAE: **Ablative Surgery and Deep Brain Stimulation for Parkinson's Disease.** *Neurosurgery* 1998, **43**(5):989-1013.
26. Hand JW: **Microwave heating patterns in simple tissue models.** *Physics in Medicine and Biology* 1977, **22**(5):981.

27. Prahl SA, Keijzer M, Jacques SL, Welch AJ: **A Monte Carlo Model of Light Propagation in Tissue.** In *SPIE Proceedings of Dosimetry of Laser Radiation in Medicine and Biology.* 1989:102-111.
28. Wang L, Jacques SL, Zheng L: **MCML—Monte Carlo modeling of light transport in multi-layered tissues.** *Computer Methods and Programs in Biomedicine* 1995, **47**(2):131-146.
29. Moller T, Trumbore B: **Fast, minimum storage ray-triangle intersection.** *Journal of Graphical Tools* 1997, **2**(1):21-28.
30. Giovanelli RG: **Reflection by Semi-Infinite Diffusers.** *Optica Acta* 1955, **2**:153-162.
31. van de Hulst HC: *Multiple Light Scattering - Tables, Formulas, and Applications.* New York: Academic Press; 1980.
32. Gardner CM, Welch AJ: **Improvements in the accuracy and statistical variance of the Monte Carlo simulation of light distribution in tissue.** In.; 1992:400-409.
33. Weakliem HA, Redfield D: **Temperature dependence of the optical properties of silicon.** *Journal of Applied Physics* 1979, **50**(3):1491-1493.
34. **Phase Change** [<http://www.comsol.com/model/phase-change-474>]

APPENDIX A VOIDSIM USER MANUAL

A.1 Preface

This manual is meant to serve as a companion to VOIDSim software. The software itself has a built-in tutorial that will serve to outline the program's basic operation. This manual may be used as a resource to fully understand software use, including its features and limitations. This may also be used as a support reference during troubleshooting.

The manual is divided into several sections, based on the feature contents of each user-interface screen/page. To access information about a specific part of VOIDSim, use the Table of Contents to identify the location of information about the specific page you need help with. The section names correspond with the labels in the navigation tree in VOIDSim, which is located along the left side of the window in which the program operates.

Further information about the use of VOIDSim software can be found in the HELP section of the program.

A.2 VOIDSim

Variable Optical Irradiation Distribution Simulation (VOIDSim) is a computer program that is able to simulate the thermal response of a system to optical irradiation. Applications of this program are varied and numerous. A researcher may be interested in determining where light is absorbed inside a tissue, or a manufacturer might want to determine how much silicon wafers heat while cutting them with lasers.

VOIDSim has the ability to use an arbitrarily-shaped geometry and to trace the light that propagates through that geometry, with all its accompanying scattering and absorption events. Furthermore, VOIDSim can accept optical properties that vary with temperature, allowing a more accurate simulation of processes that undergo large changes in temperature, and hence, optical properties.

VOIDSim requires the user to know all the related thermal and optical properties for the system which they wish to consider. Once these parameters are known, the user is presented with a user-friendly interface to accept these parameters, and to generate desired results.

The current version of VOIDSim (2.1.1) can model optical irradiation absorption, fluence, diffuse reflections, transmission of light, and ray tracing. In addition it can model heat transfer, including bioheat and phase changes.

A.3 System Requirements and Recommendations

The only requirement is that VOIDSim must be installed on top of an existing Microsoft Windows operating system.

VOIDSim requires intensive computation, and as such will benefit from fast, modern (2014) processors. In general, a faster clock rate will improve performance. In addition, VOIDSim fully utilizes multi-core CPUs, and doubling of processor cores roughly translates to halving of required processing times (twice as fast).

Depending on the simulation, VOIDSim can require large amounts of RAM. The detail of a simulation is only limited by the amount of physical RAM available to the program. 4 GB or more of RAM is recommended.

VOIDSim only uses a computer's GPU for the user-interface, and does not leverage its power in the actual simulation. This may change in future versions of VOIDSim software.

A.4 Installation/Uninstallation of VOIDSim

The VOIDSim installation package comes with two files and one folder/directory in the root directory. These three items may be zipped into a single *.zip file, in which event the zip file should be extracted before proceeding. To install VOIDSim on your local machine, simply open the file titled "setup". Installation will proceed with limited user-input from this point. Your computer may prompt you to download additional files to update your Microsoft .NET framework installation.

An icon will be created on your desktop, through which you may enter the program.

To uninstall VOIDSim, use the program management facility, located in the Windows Control Panel. Updating VOIDSim with the current version does not require uninstallation first.

A.5 User Interface

VOIDSim contains three vertical panes of information, and several pages which each contain these three panes. The leftmost pane is how you navigate VOIDSim, and will take you to that icon's respective page. The center pane is typically where user input is done. The rightmost pane is information (written/visual) about either your simulation or about the page which you are currently viewing.

In addition to the navigation in the leftmost pane, there is a menu toolbar across the top of the leftmost pane.

A.5.1 Menu Toolbar

The menu toolbar contains three choices: "FILE", "REFERENCE", and "HELP"

"FILE" presents you with options to manage your simulation. Within "FILE", there is "New", "Open...", "Save As...", "Save...", and "Exit". "New" allows you to either reset the simulation ("FILE > New > Simulation...") or create CAD geometry ("FILE > New > Basic Geometry..."). "Open..." allows you to open a previously saved simulation. "Save As..." and "Save..." will save the current simulation either with a new filename, or with the existing filename, respectively. "Exit" exits the VOIDSim program.

"REFERENCE" contains sample simulations that the user can load. The sample simulations can be a useful reference for those new to VOIDSim. The built-in simulations are able to be modified by the user.

“REFERENCE” also contains links to the text of the code used to generate post processing results in 3rd party software (MATLAB and Scilab). The code may be accessed here to see exactly how results have been generated.

“HELP” contains tools that will provide information about VOIDSim. There exists a tutorial to help a user create a simple simulation, a list of assumptions and limitation of VOIDSim, and links to report errors in the program, or view information about the current version of the program.

A.5.2 Model Creation

The start of any VOIDSim simulation is a solid three dimensional model. This three dimensional model is defined as a set of triangle indices that form the surface of the solid model. VOIDSim uses the binary STereoLithography (STL) file format to define its models. Most commercial CAD software allows for exporting a model in the STL format. This is most often done through an “export” or “save as...” menu choice.

Tips for exporting STL models from existing CAD geometries:

- Export/save your model as a **binary** STL file (not ASCII)
- Each domain requires a separate STL file. For example, if your system consists of three distinct layers in a geometry, there should be three STL files
- Make a note of the units that your model was created/exported/saved in

- The resolution of your model will directly impact the accuracy and speed of VOIDSim execution, with high-resolution leading to longer execution time, with (potentially) improved result accuracy
- Make a note of which file corresponds to which material in VOIDSim
- You may wish to translate the model to positive geometric space (no negative coordinates), although this is not necessary

In the event that you have a simple system to model, you may use the built-in STL creator. Note that the built-in STL creator can only generate rectangular prisms.

A.5.3 Create Basic Geometry

To start the basic geometry creator, go to “FILE > New > Basic Geometry...”. Alternatively, you can select the “Create Basic Geometry...” button in the “Geometry” page. After you open the geometry creator you are presented with three vertical panes. The leftmost pane is where you give your geometric inputs. The center pane will give you the three standard projected views (XY, XZ, and YZ planes) of your geometry, with each color representing a distinct domain. If you have not yet created any geometries, the center pane will remain blank. The rightmost pane shows the three dimensional view of your model, as it currently exists, with one color for each domain. If you have not yet created any geometries, then the VOIDSim logo will be in this pane. Clicking on the rightmost pane will display the three dimensional model display in a new window, which you can manually rotate.

Domains are defined as rectangular prisms (each face of the solid is a rectangle). Each rectangular prism is defined by specifying its size and location. Once you define the origin (Cartesian X, Y, and Z position) of the new domain (using the “Box Origin” inputs in the leftmost pane), the “Box Size” inputs define how the sides of the box will extend from that point, in each of the noted Cartesian directions. Note that the size values may be negative, indicating negative direction. Boxes cannot be rotated, and existing geometries cannot be imported. After you indicate the size of the box, click “Add Box to Geometry” to add the domain to your system. This option will only be available if your box size is non-zero in each direction.

You may remove erroneous boxes by selecting them in the “Geometries” list, and then by selecting “Remove Selected Box”.

Once you have created all desired domains, then you can export your model to an STL file which VOIDSim can use. The “File Identifier” will preface each of your saved domain files, for your reference.

When ready, select “Save Geometries...” to save your geometry as a series of STL files. The program will ask you where to save your files. After saving the files, VOIDSim will give you the opportunity to directly load the created geometry into your VOIDSim simulation.

A.5.4 Simulation

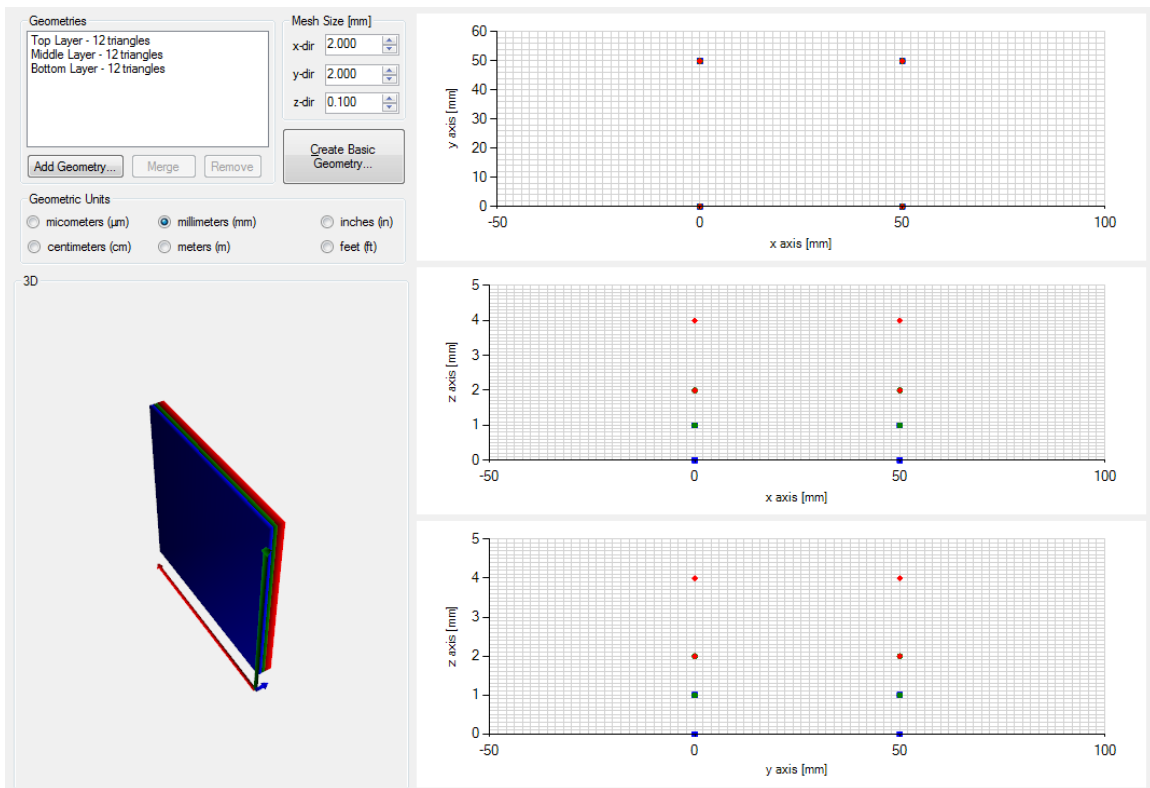
The simulation page is accessed by selecting the “Simulation” icon in the VOIDSim leftmost pane. Selecting this page allows the user to give a name to their simulation (“Simulation Name”), define the directory on the computer where simulation results will be saved (“Solution Directory”), and to select the physics they wish to include in the simulation (“Simulations/Outputs”). In addition to selecting the various available physics, the user also can choose which optional outputs are stored in “Simulations/Outputs”. Instructions for “Simulations/Outputs” are given in the rightmost pane of the “Simulation” page. Selecting the checkboxes will include the selected physics/option.

A.5.5 Geometry

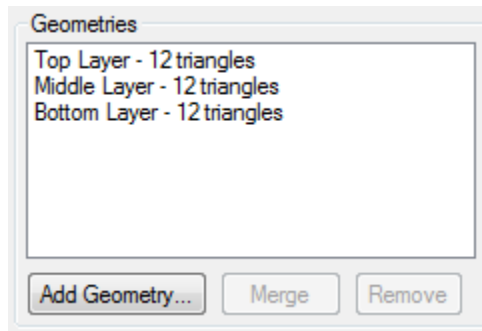
The geometry page is accessed by selecting the “Geometry” icon in the VOIDSim leftmost pane. The first thing to do on this page is to import your system geometry from a CAD file.

To add a CAD model to VOIDSim, first the file must be saved in STL file format. Once you have the STL file collection (one file for each domain) you may import your geometry in VOIDSim. This is done by clicking the “Add Geometry...” button in the center pane. Clicking this opens a file-select dialog, where you may select one (or all) of your STL files, representing your system. Multiple files may be selected by holding the “Ctrl” or “Shift” keys while selecting the files with your mouse. When you have each desired file selected, click “Open”. This imports your files into VOIDSim. If all goes well, your geometry

will be displayed in the rightmost pane (projected views) and in the bottom of the center pane (three dimensional view). In each view, each domain is represented by a distinct color. Clicking the three dimensional view opens a separate window in which you can manipulate the view of your system.



In addition to the views, your geometries, with their names will be displayed in the “Geometries” list. Each name is appended with the number of triangles which define their exterior. Selecting a geometry from the list will update your projected and three dimensional views to show just the selected geometry (or geometries, in the case of multiple domains being selected).

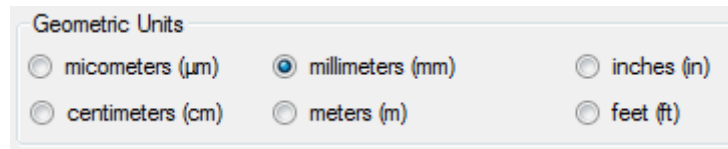


Also, in addition to the views and names, new pages for each of your domains will be available in the leftmost pane. You can set the properties for individual domains in those pages.

In the “Geometries” list in the center pane, you can continue to add additional geometries, remove or rename existing geometries, or merge geometries. Merging geometries will assign all physical properties of the merged geometries to be identical. To do this, select multiple geometries from the list (holding the “Shift” or “Ctrl” key) and click “Merge”. You are then asked to select the parent domain, or rather, the domain which you will specify properties for, which the other merged domains will share. After this is done, the “Geometries” list will be updated to reflect which domains have been merged with others, by appending their names with “(merged)”.

It is important that you match the units of your model with those used in the model’s creation/export. This is done with the selection of the appropriate units in the “Geometric Units” field in the center pane. If your geometric units do not match one of

the available choices, you must alter your CAD file, as this cannot be reconciled in VOIDSim.



The mesh size defines the resolution of your system. The size of your mesh determines how many nodes will be evaluated during execution of the simulation, so it is important to use a fine enough mesh to display the details you need, while also keeping mesh size large enough, so as to avoid out-of-memory issues and to minimize the time it takes to run your simulation.



As a visual aid, as you update the mesh size, the mesh will overlay the projected views of your model with gray lines. If any of your projected views have a solid gray background, it is likely your mesh is too fine. Conversely, if any of your projected views has a solid white background, it is likely your mesh is too coarse. Mesh size is changed through the user-interface in the center pane. Mesh size is defined in the same units in which your model is defined.

Notes on mesh size:

- The mesh size has no bearing on the accuracy of optical irradiation distribution (for constant optical property domains), however the distribution resolution directly impacts the accuracy of heat transfer
- When optical properties vary with temperature the accuracy of optical propagation will be impacted by the mesh size
- When optical properties can vary with temperature the accuracy of optical propagation results will be dependent on the mesh size
- The minimum mesh size that can be used is directly affected by the available memory to the computer, with as many as 160 bytes of information needed for each mesh intersection (node)

A.5.6 Domains

After a domain is imported into VOIDSim, a page for each domain will be created and displayed in the leftmost pane. Selecting these pages will allow you to define the physical properties for the selected domain.

On each domain page you will be presented (in the center pane) with the physical properties that need definition for the physics that you selected in the “Simulation” page. Only those properties pertinent to the selected simulations will be present, and the properties will be updated as the simulation selections change.

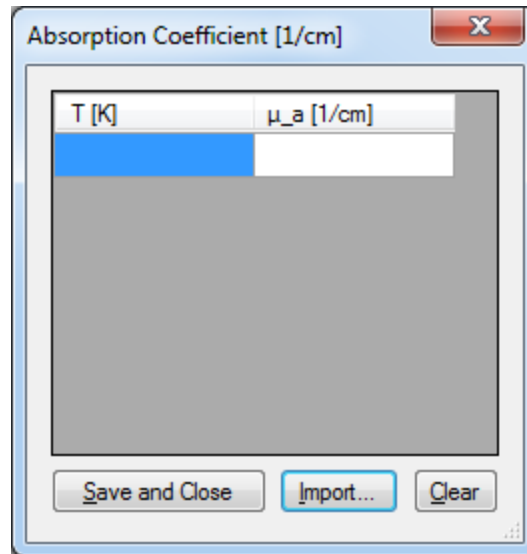
At the top of the center pane, the domain’s name is displayed, along with the options of saving the current set of properties, or loading a previously-saved property set.

Most property sets have three choices for their definitions: “Table”, “Constant”, or “Above/Below Transition”. Select “Table” if you wish to define the particular properties in a look-up table. “Constant” should be selected if the property never changes with respect to temperature. “Above/Below Transition” should be selected if you wish to define discrete property values when the domain’s local temperature is above or below a certain threshold temperature (“Transition Temperature”). Note that not all selections may be available due to choices made in the “Simulation” page and/or limitations in VOIDSim. Entering values in the “Constant” or “Above/Below Transition” fields is trivial, while entering a table is not as straight forward.

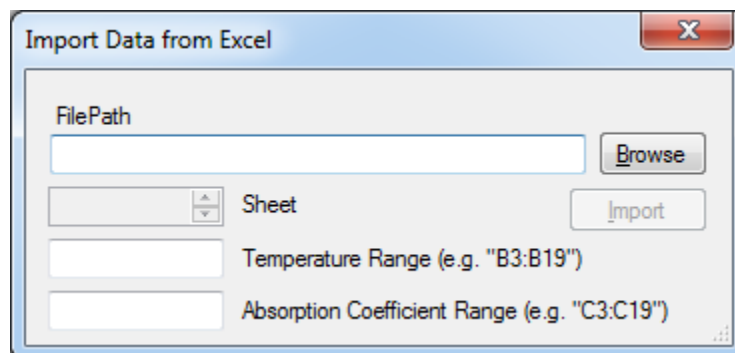
Tables that are not yet defined are indicated with red text. As the tables become defined, the text will turn green, and the simulation is allowed to be evaluated.

Optical Properties	Table	Constant	Below Transition	Above Transition
Absorption Coefficient [1/cm]	<input checked="" type="radio"/> f(T)	<input type="radio"/> 10	<input type="radio"/> 0.89	<input type="radio"/> 0.89
Scattering Coefficient [1/cm]	<input checked="" type="radio"/> f(T)	<input type="radio"/> 90	<input type="radio"/> 289	<input type="radio"/> 289

A table is defined by clicking the button for the respective table. It opens a new window that allows the definition of a series of temperatures and property values. Temperature values may not be repeated, but property values may. You can clear the contents of the table by clicking “Clear”, or you may save the values with “Save and Close”. You may also create your property tables in Microsoft Excel, and import those values directly into your table.



Importing values is done by clicking “Import...”. The import dialog will ask for the location of the excel file you wish to get table data from. Once a file is specified, the sheets of the file will be presented in a list. Select the correct sheet from the list, and specify the values’ data ranges as shown in the dialog.

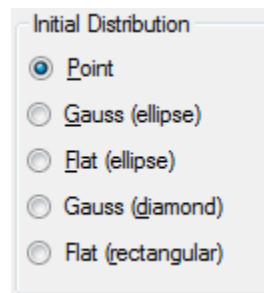


A.5.7 Optical Distribution

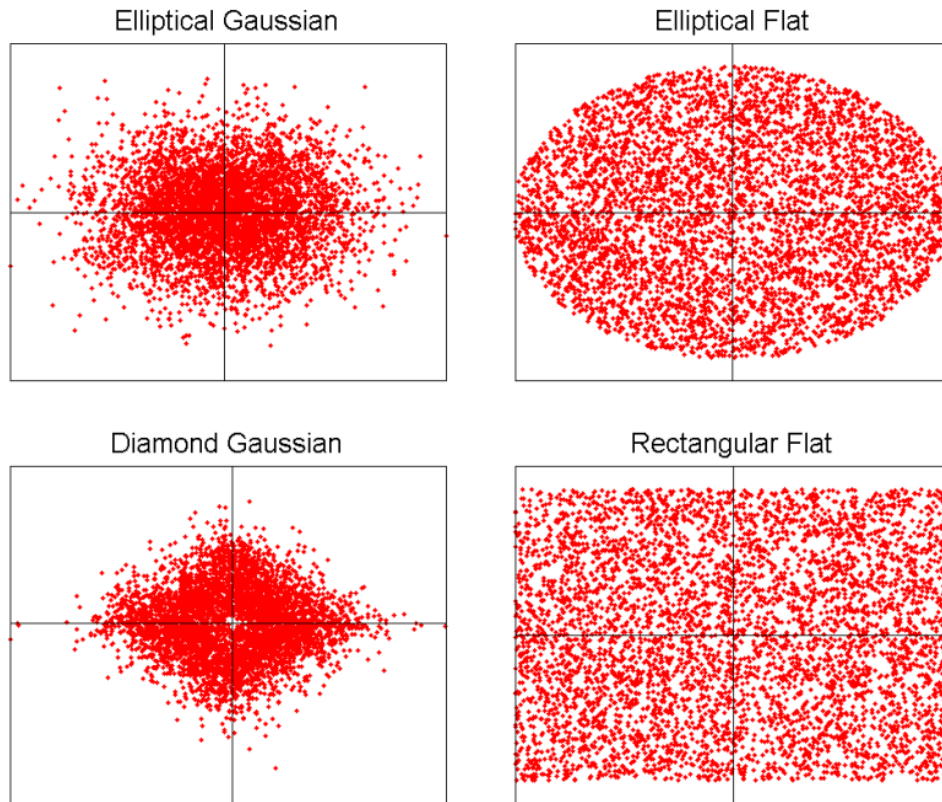
The optical distribution page is accessed by selecting the “Optical Distribution” icon in the VOIDSim leftmost pane. This page contains links to the “Source Geometry”, “Source Profile”, and “Adjustments” pages.

A.5.8 Source Geometry

The source geometry page is accessed by selecting the “Source Geometry” icon in the VOIDSim leftmost pane. This page defines the physical geometry and orientation of the incoming optical irradiation.



The initial distribution describes how the incoming irradiation first is distributed across its cross-section, perpendicular to its principal direction. “Point” indicates that all irradiation originates from the same point in space, without any horizontal distribution. It is equal to a beam radius of zero. “Gauss (ellipse)” indicates a normal distribution that is elliptical in shape. “Flat (ellipse)” indicates that there is a uniform distribution of rays in the orthogonal plane. The last two choices are similar to the elliptical choices, with the difference that the distribution is in the shape of a rectangle, or diamond.



“Angle” defines how the irradiation is diverging or converging. “Collimated” indicates that all of the irradiation is moving in the same direction. Selecting “Divergence” allows the user to select a divergence angle, which determines a “cone” which all incident irradiation lies inside. Defining the X, Y, and Z coordinates of a “Convergence Point” directs all irradiation from its origin towards the convergence point.

Angle

Collimated

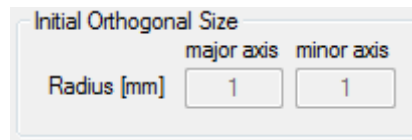
Divergence [deg] 30.0

Convergence Point [mm]

0 0 0

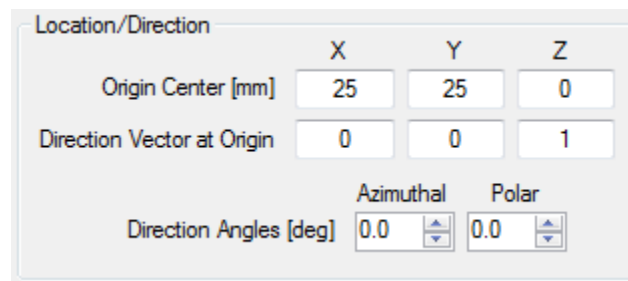
X Y Z

The “Initial Orthogonal Size” refers to the size of the cross section of the irradiation in the plane which is orthogonal to the principal direction. The major/minor axes define the size of the sides of the rectangle for rectangular distributions, or diameters for ellipses.



A dialog box titled "Initial Orthogonal Size" with two input fields. The first field is labeled "major axis" and the second is labeled "minor axis". Below these fields is a label "Radius [mm]" followed by two input boxes, each containing the value "1".

The location at which the irradiation originates is defined in “Location/Direction”, as well as the principal direction of the beam.



A dialog box titled "Location/Direction" with a table for Cartesian coordinates and two spinners for angles.

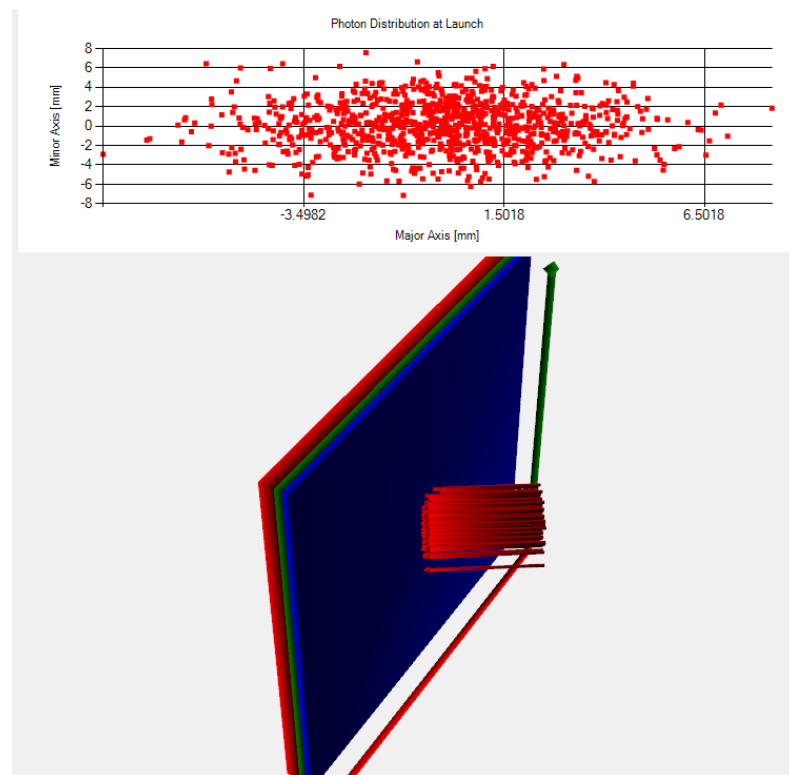
	X	Y	Z
Origin Center [mm]	25	25	0
Direction Vector at Origin	0	0	1

Direction Angles [deg]

Azimuthal	Polar
0.0	0.0

The “Origin Center” is the center of the origin of the distributed beam, in Cartesian coordinates. The “Direction Vector at Origin” is the principal direction vector of the irradiation. Alternatively, the user may define the principal direction using the azimuthal and polar angles of the initial direction. The azimuthal angle is defined as the angle the irradiation makes with the positive x axis, while the polar angle is the angle the irradiation makes with the positive z axis.

As you update your source geometry, it will be displayed and updated in the rightmost pane. The top part will show an orthogonal projection of the irradiation distribution, while the lower portion displays a three-dimensional view of your model, with the incident irradiation displayed as a group of arrows.

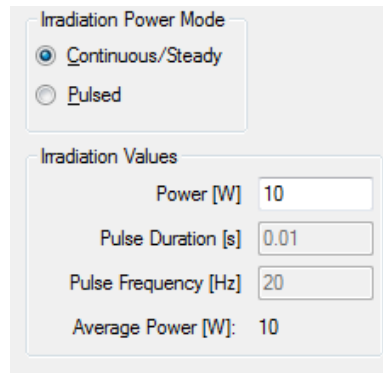


A.5.9 Source Profile

The source profile page is accessed by selecting the “Source Profile” icon in the VOIDSim leftmost pane. This page defines the temporal (time-dependent) properties of the incoming optical irradiation.

“Irradiation Power Mode” has two choices for incoming optical irradiation. The first is continuous, or steady power, meaning that incoming irradiation does not vary with

time. The user may also choose a pulsed source, which treats incoming irradiation as a square wave function.



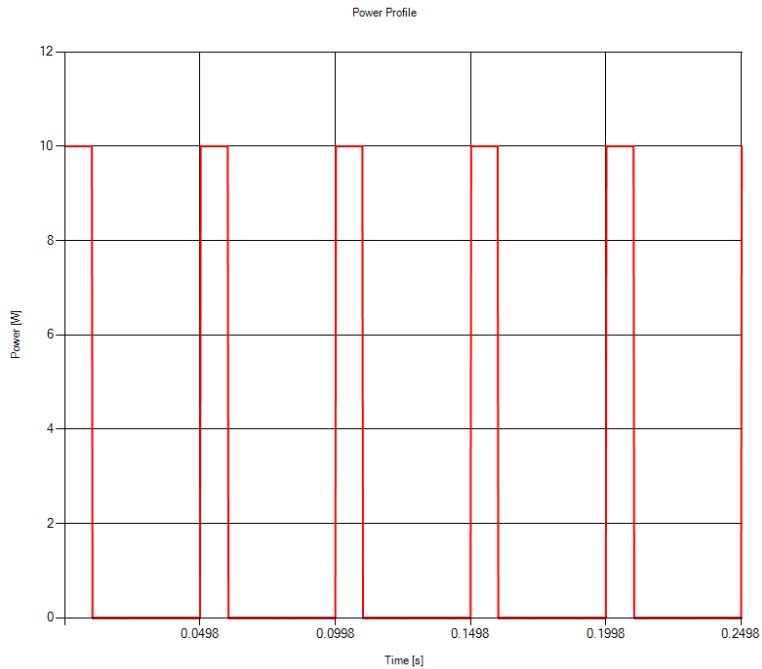
The image shows a software interface for configuring irradiation parameters. It is divided into two sections: "Irradiation Power Mode" and "Irradiation Values".

Irradiation Power Mode: This section contains two radio buttons. The first, "Continuous/Steady", is selected with a blue dot. The second, "Pulsed", is unselected.

Irradiation Values: This section contains four input fields and a calculated value:

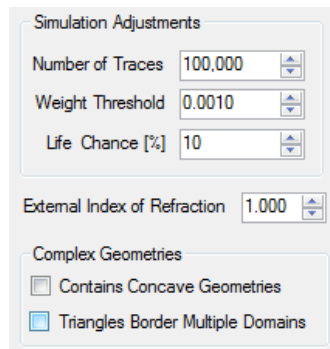
- "Power [W]" is a text box containing the value "10".
- "Pulse Duration [s]" is a text box containing the value "0.01".
- "Pulse Frequency [Hz]" is a text box containing the value "20".
- "Average Power [W]:" is a label followed by the value "10".

Under “Irradiation Values” you will define the power of your irradiation source **when it is active**. This is power output during a pulse for a pulsed source. If a pulsed source is chosen, the user will define the pulse characteristics in the section as well, including the pulse duration and frequency. As an aide to the user, the average power delivered to the geometry will be displayed. On the rightmost pane a representation of your irradiation source power profile will be displayed.



A.5.10 Adjustments

The adjustments page is accessed by selecting the “Adjustments” icon in the VOIDSim leftmost pane. This page allows for manipulation of basic Monte Carlo simulation parameters, and allows the user to toggle geometric restrictions.



“Number of Traces” refers to the number of simulated photons that will travel through your geometry. The greater the number, the better the distribution accuracy, at

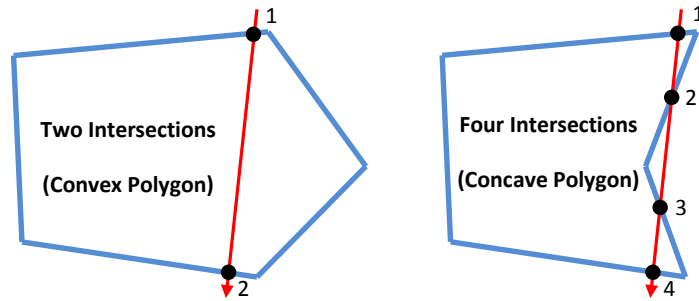
the expense of speed. If the simulation is being performed to merely show the path of representative photons, this value may be set low (less than 100), otherwise it should remain within an order of magnitude or two of its default value.

“Weight Threshold” refers to when a photon is considered to have given up all of its significant life. This is a fraction of one. Once a photon’s weight drops below the threshold, it is terminated, and its remaining weight is donated to a pool, which the occasional photon will deplete. Changing this value may lead to enhanced simulation speeds and accuracy, although it is not normally needed to change the value.

“Life Chance” refers to the chance that a dying photon has in accessing the leftover weight pool before its termination. Changing this value may lead to enhanced simulation speeds and accuracy, although it is not normally needed to change the value.

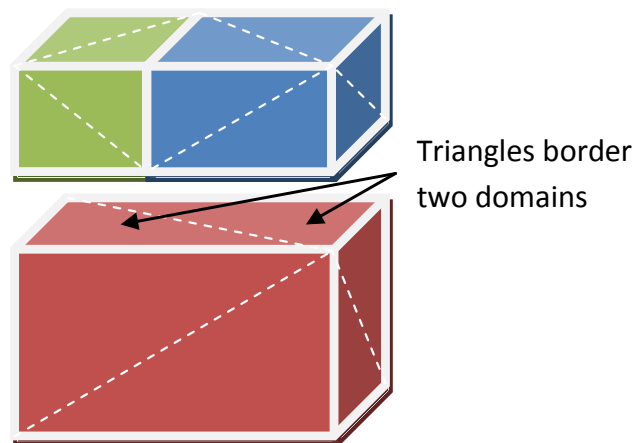
“External Index of Refraction” refers to the index of refraction of the area external to the simulation. It is by default set to 1, representing air, or a vacuum, but may be altered as needed (e.g. if your system is submerged in water).

“Complex Geometries” is an option for the user to indicate that their geometry does not meet simplified rules. Following the rules leads to increased performance of the simulation, however these rules can be overridden here to allow for more complex geometries.



The first checkbox is required if your geometries contain any closed concave polygons. That is, that **any** line drawn through your model must intersect model boundaries exactly twice (no more, no less). Keep in mind that this condition must hold in three dimensions. If more intersections are possible, then check this box.

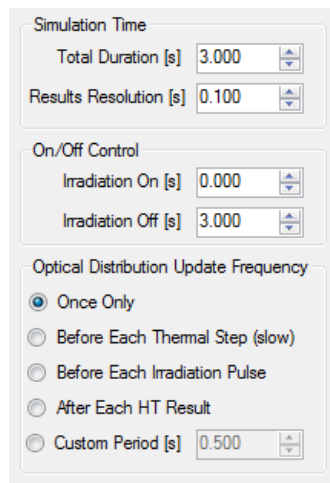
The second checkbox deals with how different domains intersect each other. The surface of each domain is created by a series of triangles. If it is possible to draw two or more lines passing through one triangle of domain A (red in the image below) into multiple adjacent triangles (blue and green), then your domain borders multiple domains, and this checkbox must be marked.



A.5.11 Heat Transfer

The Heat Transfer page is accessed by selecting the “Heat Transfer” icon in the VOIDSim leftmost pane. This page defines the duration of heat transfer simulation, and allows the user to control when optical irradiation hits the system, and how often the optical distribution is updated.

In the current version of VOIDSim, there are not many options for modifying the nature of heat transfer on this page. Boundary conditions are fixed, and borders between domains are treated as continuous.



The screenshot shows a control panel for the Heat Transfer simulation, organized into three sections:

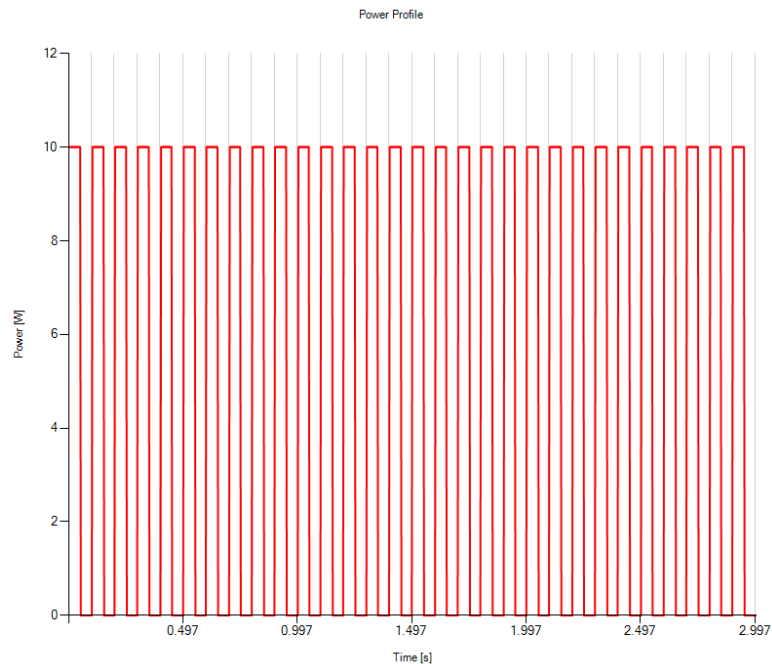
- Simulation Time:**
 - Total Duration [s]: 3.000
 - Results Resolution [s]: 0.100
- On/Off Control:**
 - Irradiation On [s]: 0.000
 - Irradiation Off [s]: 3.000
- Optical Distribution Update Frequency:**
 - Once Only
 - Before Each Thermal Step (slow)
 - Before Each Irradiation Pulse
 - After Each HT Result
 - Custom Period [s]: 0.500

What can be changed is the total duration of heat transfer simulation, when the irradiation source starts and when it stops, and how often heat transfer is coupled with optical distribution.

“Total duration” is the duration of time that the simulation should cover. “Results Resolution” controls only how often heat transfer results are saved to the hard disk, as

the program determines how often to update the heat transfer, based on numerical stability.

“On/Off Control” determines when an irradiation source should start impacting the system, and when it should stop. The values chosen here will update the rightmost panel, which displays the irradiation profile over the duration of the simulation. The gray lines present in this representation indicate the points in time in which a result will be saved to the hard disk.



There are several choices for the frequency at which the optical distribution is updated. The first choice, “Once Only,” only gets the irradiation profile once, before the start of heat transfer. This is appropriate to use if constant optical properties are used, as the optical distribution will not change with changes in temperature. In fact, if constant

optical properties are used, the choice made by the user for “Optical Distribution Update Frequency” will not be taken into consideration.

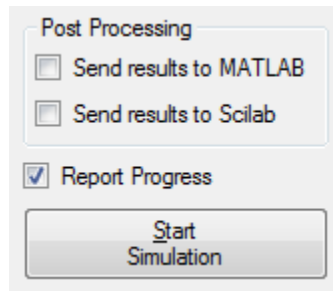
“Before each thermal step” will give the user the greatest accuracy of results, as the simulation will first calculate optical distribution, then heat transfer for a single incremental time step, then it returns and updates the optical distribution, and so on. This requires much computer processing, and can be very slow. The optical distribution is only recalculated when the irradiation is active.

“Before each irradiation pulse” recalculates the optical distribution before each new laser pulse, for pulsed irradiation sources, or before the start of a delayed-onset continuous irradiation source.

“After each HT result” updates the optical distribution on a schedule that corresponds with the user-defined “Results resolution”. “Custom period” is identical, but the user may specify a unique update schedule.

A.5.12 Run Simulation

The run simulation page is accessed by selecting the “Run Simulation” icon in the VOIDSim leftmost panel. This page allows the user to set basic options for post processing and progress reporting. It is also how a user will initiate a simulation being evaluated.



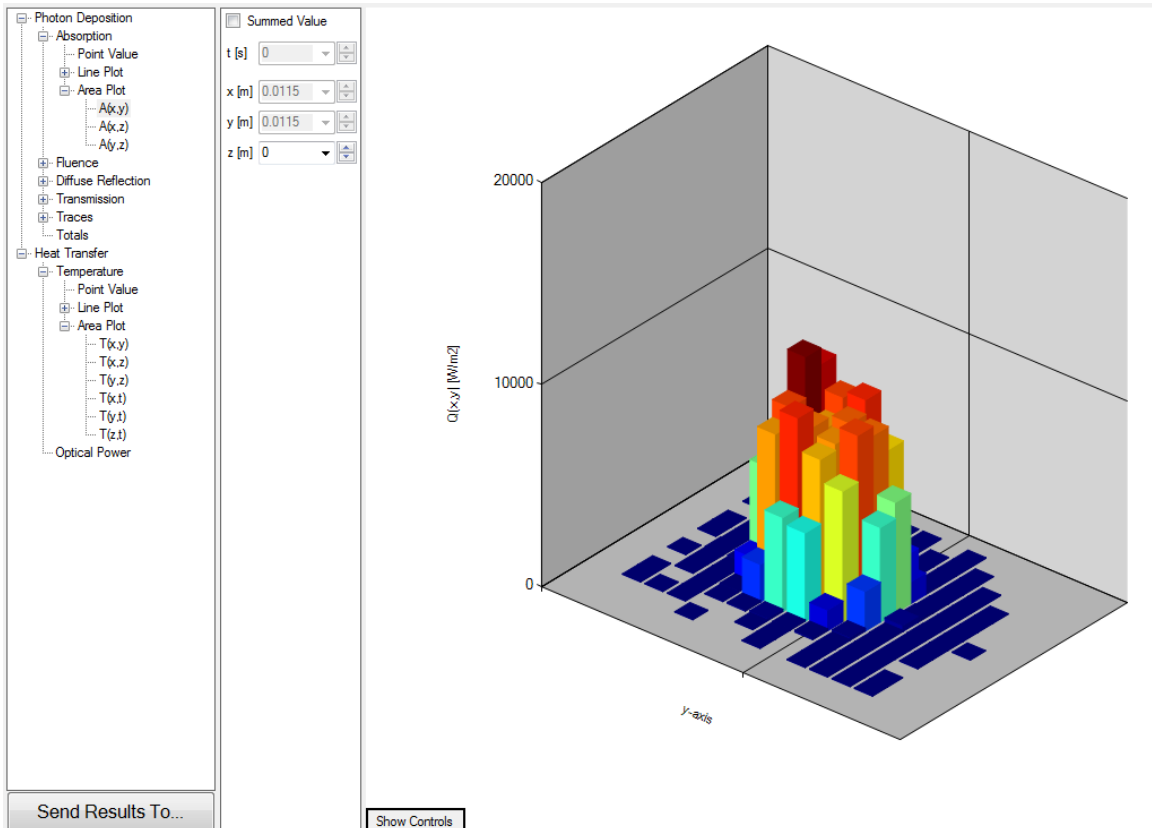
Sending results to MATLAB/Scilab will open the selected program(s) after the simulation is complete, and will initiate post processing analysis and visualization. The programs will only be opened if installed on the computer along with VOIDSim. “Report Progress” allows the user to indicate if simulation progress will be reported as it goes. This is at the expense of execution speed, but aids in providing estimated finish times, among other things.

Clicking the button “Start Simulation” starts the simulation and opens a new dialog which indicates simulation progress (if enabled). After completion of the simulation, the user is taken to the results page.

A.5.13 Results

The results page is accessed by selecting the “Results” icon in the VOIDSim leftmost pane. This page displays basic results to the simulation. For more advanced/custom results, perform post processing analysis and visualization in a 3rd party program (e.g. MATLAB, Scilab).

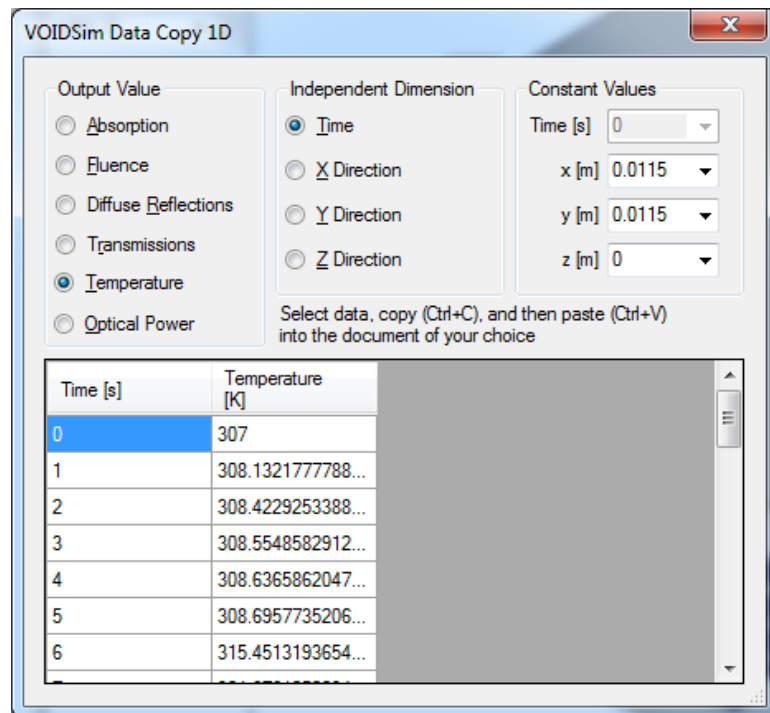
Results will only be available after running the simulation, and only results for those simulations the user included (e.g. heat transfer, optical distribution, photon tracing, etc.) will be available.



The center pane will have a selection tree available to choose the results you wish to display, as well as which dimensions of those results you wish to display. The second column in the center pane is dedicated to indicating the location that the result data comes from. For example, the displayed data above is for an area plot of the absorption, displaying the x and y axes at a constant z axis value of 0. The z axis value may be changed in the second center pane column, while the choice of displaying $A(x,y)$ is made in the first

column. The rightmost pane shows a graphical representation of the data, with ability to rotate view for three dimensional data.

The results are meant only to provide insight into the behavior of the solution, and are not intended to be used in scientific analysis or presentation. To get the raw data and to perform customized post processing, the user may choose to automatically send result data to MATLAB or Scilab programs for post processing (see Run Simulation section), or can export data using the “Send Results To...” button in the results page. As an additional option, the user can create one-dimensional arrays of data for export to spreadsheet programs (e.g. Microsoft Excel) using this button (pictured below).



A.6 Additional Help

If you are experiencing unresolved issues, or are experiencing unexpected behavior, you may contact the software's creator for additional help:

Adam B. Slade

aslade@engr.ucr.edu

Suggestions and bug-reporting are always welcome, and serve to improve future versions of VOIDSim.

A.7 Glossary

Domain	A discrete geometric region which defines a region where all properties are homogeneous. Domains are defined in VOIDSim with a STL file.
STL	STereoLithography File. A file which contains the vertices of the triangles which make up the outside surface of a solid geometry. Used to define geometries in VOIDSim
System	The collection of all geometric regions in the simulation. Systems are defined in VOIDSim with a collection of STL files (domains).
VOIDSim	Variable Optical Irradiation Distribution Simulation. A Monte Carlo simulation for determining the thermal response to optical irradiation, where optical (and thermal) properties may vary with temperature.
External Domain	The area external to the system, where irradiation and heat transfer are not considered.
Irradiation	Optical electromagnetic radiation which is incident upon the system.
Triangles	Three points in three dimensional Cartesian space which define a surface. A collection of triangles forms a domain.
Principal Direction	The direction in which the irradiation is initially aimed.
Mesh	The lines which form the edges of the rectangular prisms (nodes) which make up each domain

Node The “building blocks” of a VOIDSim model. The edges of the node are the mesh lines. Each node has homogenous properties (including temperature) at all points in time.

